Heliyon 10 (2024) e26696

Contents lists available at ScienceDirect

Heliyon

journal homepage: www.cell.com/heliyon

Review article

Alkali activated materials applied in 3D printing construction: A review

Maria Júlia Bassan de Moraes [a,*], Ester Yukimi Nagata [a], Afonso José Felício Peres Duran [a], João Adriano Rossignolo [b]

[a] Post-Graduation Program in Material Science and Engineering, Faculty of Animal Science and Food Engineering, Universidade de São Paulo (USP), Brazil

[b] Department of Biosystems Engineering, Faculty of Animal Science and Food Engineering, Universidade de São Paulo (USP), Brazil

ARTICLE INFO

Keywords:
Review
Additive manufacturing
Alkali activated materials
Geopolymer

ABSTRACT

This study aims to contribute to the promising field of alkali-activated materials (AAM) used in 3D printing for construction. Presented as a comprehensive review, the research provides valuable insights for researchers within and beyond the field. The study focuses on identifying prevalent research trends and accessing pertinent information on materials, methodologies, and parameters of interest. The study commenced with a bibliometric analysis of 55 carefully selected publications, followed by an in-depth review of these articles categorized into extrusion-based and powder-based systems. Emphasis was placed on the materials used, methodologies employed, and key findings from these studies. The bibliometric analysis unveiled prevalent keywords, their relevance in the field, highly cited articles, and collaborative networks among researchers. The most influential countries in terms of publications are Australia, China, and Singapore. The review highlighted commonly used materials and their potential impacts on large-scale applications of AAM, exploring how various precursors, activators, additives, aggregates, and reinforcements shape the properties of printed AAM, featuring innovative approaches with alternative materials. The methodologies employed in these studies and trends in characterization were outlined, due to the absence of standardized tests for materials in 3D printing applications. The study emphasized how material properties vary concerning production processes, printing parameters, curing methods, and post-treatment, outlining advancements in material characterization necessary for achieving a printable mix design. Through the analysis of these 55 articles, key scientific challenges and hurdles in large-scale applications were identified, suggesting potential focal points for further studies. In summary, AAMs exhibit substantial uniqueness and complexity due to their diverse material composition, resulting in varying properties in both fresh and hardened states. However, this diversity also signifies the adaptability of AAMs to diverse equipment, construction techniques, and desired specifications, showcasing their potential to revolutionize traditional construction by integrating technology and sustainability.

1. Introduction

In the past decade, the concept of Industry 4.0 emerged, initially intended to describe the digitization of manufacturing processes,

* Corresponding author.
E-mail address: maju.bamoraes@usp.br (M.J. Bassan de Moraes).

https://doi.org/10.1016/j.heliyon.2024.e26696
Received 29 November 2023; Received in revised form 16 February 2024; Accepted 19 February 2024
Available online 22 February 2024

limited to the application of advanced digital manufacturing, such as 3D printing, modeling, and virtualization only in factories. However, there has been a recent change of perspective regarding Industry 4.0, expanding its application throughout the production chain, and promoting high digitization, automation, and virtualization in different sectors and areas [1].

Therefore, civil construction has also been influenced by the Fourth Industrial Revolution, particularly in construction methods, through the utilization of additive manufacturing. Additive manufacturing is defined by ISO/ASTM as the "process of joining materials to make parts from 3D model data, usually layer upon layer, as opposed to subtractive manufacturing and formative manufacturing methodologies" [2].

In construction, the most common printing process is extrusion-based, where structures are created from the bottom up through an extrusion nozzle, overlapping layer by layer [3]. Fig. 1 schematically shows the extrusion 3D printing process, in which the filament is extruded and deposited layer by layer on the substrate.

However, there are also studies using the powder-based technique for application in civil construction [4]. The method consists of spreading a thin layer of powder and then blasting the binder (liquid) at specific points [5]. The binder droplets are selectively applied to the powder layer by a printhead, causing adhesion between the powder particles. The structure is constructed by repeating the steps described [6]. Fig. 2 (a) and (b) show this process [7].

The application of additive manufacturing in construction brings benefits such as increased productivity, technical and economic optimization, the production of geometrically more complex structures, minimal waste of materials, and greater safety, among others [8,9]. Moreover, it can present a new perspective on construction, such as in environments that are difficult to access [10,11]. It may also be able to build emergency shelters and more affordable housing [11]. The possibility of producing more complex structures or not requiring molds for construction can also mean a renewal of paradigms in traditional constructions, leading to a revolution in civil construction.

However, the constructions of the future are not only concerned with the improvement of construction methods and performance of materials but also with the environmental impact caused by them. Thus, in addition to the search for new technologies, there is also a concern with sustainability and circular economy.

The production of Portland cement, widely used in civil construction, is responsible for several environmental impacts, including high energy demand, use of non-renewable materials, and, most importantly, high carbon dioxide emissions, since its production is responsible for about 7% of global CO_2 emissions [12].

An option to replace Portland cement-based matrices is alkali-activated materials (AAMs), defined as cementing materials derived from the chemical reaction between an alkaline solution, or alkaline activator, and an amorphous aluminosilicate material, the solid precursor [13].

Alkali-activated materials are divided into three systems according to the nature of the cementing material: systems with high calcium content, with blast furnace slag being the most traditional precursor; systems with low calcium content, also called geopolymers, in this case the most used precursors are metakaolin and fly ash of Type F; and hybrid systems, which can be a mixture of the two systems mentioned or the inclusion of Portland cement in one of them or in the mixture itself [13].

Although some review articles and analyzed studies use the term "geopolymers" to refer to all systems, for a better understanding of the subject, this study will use the nomenclature that covers all systems (AAMs) to refer to the alkali-activated materials, including geopolymers.

AAMs are considered a sustainable alternative to Portland cement, partly due to the option of utilizing precursors derived from other industries that do not involve high temperatures and result in lower CO_2 emissions during production [14]. Although they have the potential to be eco-friendly, one cannot state this in a generic way regarding all AAMs, since they are an extremely diverse group of materials and their rheological, physical, mechanical, economic, and environmental characteristics vary depending on the precursor and activator used.

The required characteristics of printed materials vary depending on the printing system, type of printer, design of the printed object, desired characteristics, and printing parameters, among other factors. Therefore, the versatility of AAMs and the possibility of adapting their mix design to different properties represent a great option to be studied for 3D printing applications.

However, in addition to this variability of AAMs, it should be noted that additive manufacturing is a relatively new technology in

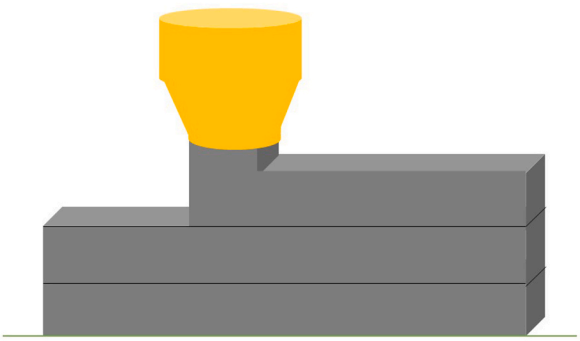

Fig. 1. Extrusion printing process.

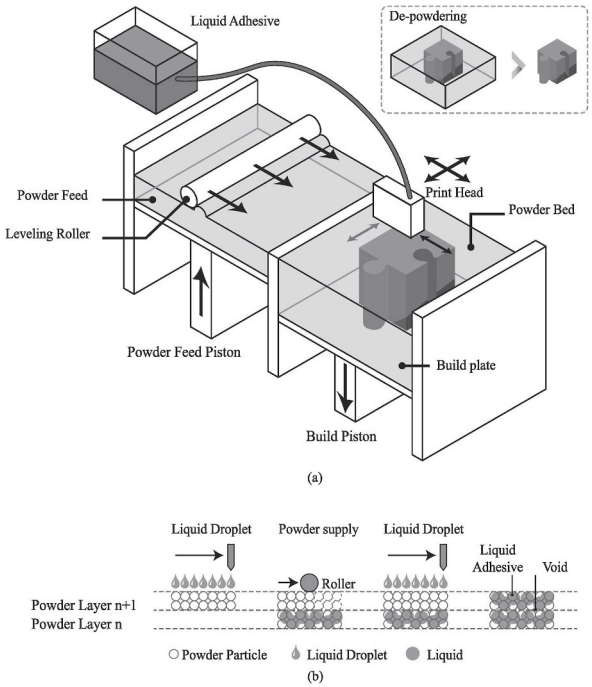

Fig. 2. Schematic illustrations of the 3D printing process for powder-based system: (a) the system, (b) powder/binder interaction between adjacent layers [7].

civil construction and many studies and improvements are still needed to widely use this technology. Thus, literature reviews are great contributors to highlight and analyze what has been produced scientifically on this topic, contributing to a better understanding and evaluation of the AAMs applied in 3D printing.

This study was designed to contribute to this promising field of research by presenting the panorama of publications and bibliometric analysis; to the best of the authors' knowledge, this is the first research doing this analysis. The selected articles were detailed, and their data was organized in figures, tables, and topics planned so that the researcher can easily identify the material, methodology, or information on results that interest them, as well as identify the source articles of this information.

This publication aims to enable readers and researchers to identify trends in previously published research. This will assist in understanding the current state of the art and contribute to the standardization of parameters and analysis.

2. Methods

Although this review is not a systematic review per se, the authors followed certain procedures based on studies presented by Lima et al. [15] and Rossignolo et al. [16]. Thus, a protocol was established for assembling a set of selected data.

To conduct this review, an electronic search was carried out across reputable databases in the scientific community with extensive coverage across diverse academic areas. The databases used were Scopus and Web of Science. The period defined for the research is the last 7 years (2017–May/2023), emphasizing recent research articles.

The search performed consisted of three phases: Research; Screening; and Eligibility and Final Analysis. The methodologies employed were based on the approaches outlined by Tinoco et al. [17], Schuldt et al. [11], Shamseer et al. [18], and Silva and Sanjuàn [19].

In this stage of the research, five filters were applied using Boolean operators and special characters along with the specific field labels of each database. Table 1 shows schematically the number of articles found in each filter application.

In the 1st filter, the search was carried out in a general way, searching for the terms related to 3D printing in all fields (title, abstract, keywords, introduction, etc.), using asterisks to include singular, plural, and variation of keywords (3D Print*, Additive

Table 1
Sequence of filters and results of the review identification phase.

Filters/Databases	3D Printing	Civil Construction	Alkali Activated Materials	Date (2017–2023)	Language (English)	Consolidated base
	1st Filter	2nd Filter	3rd Filter	4th Filter	5th Filter	
Web of Science	12,026	114	18	17	17	59 (4 duplicates)
Scopus	62,464	1882	162	45	42	

Manufacturing*). In the 2nd filter, the search was carried out within these results (1st filter), looking for studies in the area of civil construction that use 3D printing in some way, by the use of quotes to avoid terms, variations, and abbreviations (“Automation in Construction”*, “Concrete Prin”*, “3DCP”*, “Additive Construction”*, “Contour Crafting”*, “Civil Construct”*, “Construct Technolog*“, “Build* Technolog*“). The 3rd filter was used to find studies on alkali-activated materials with relevance within the construction area (“Alkali Activated Materials", “Alkali Activated Binders", Geopolymer*, “Geopolymer Concrete", Alkaline Activated, “Alkali-Activated"). The 4th and 5th filters aimed to filter the most recent studies in the past 6 years in English; then a quick reading was carried out to exclude duplicate studies, totaling a consolidated base of 55 studies.

In the screening and eligibility phase, the selection was made by reading the abstracts, introduction, and conclusions, to verify whether all studies under the scope of the review. The final analysis was the complete reading of the studies, culminating in a sample of 55 articles referring to the use of 3D-printed alkali-activated materials in civil construction.

Table 2 describes in detail the inputs and outputs of each step, defining the articles selected for the final bibliometric analysis of the review of this study.

The 55 articles were inserted in the VOSviewer software version 1.6 18 for the representation of the data by two-dimensional visualizations and maps. An analysis of the results was carried out by eliminating singular/plural terms and duplicate keywords. For instance, terms like “3D printing," “3D-printing," “3-dimensional additive manufacturing," “additive manufacturing," “additive construction," “3D printed geopolymer," and “3D concrete printing" were unified into the term “additive manufacturing. The terms Alkali activated concrete, Alkali activated material, and Alkali activation have been unified into the term Alkali activated materials. In the process of developing the maps, many terms were unified to highlight some pertinent analyses in that data set; for example, the terms referring to mechanical and rheological properties and tests were grouped to show on the map which keywords are most used in studies on 3D printing with AAMs.

This study is divided into three stages. In the first part, the bibliometric analysis of the selected publications will be presented.

The second part consists of displaying information and analyses of articles on the topic. Thus, the materials and methodologies covered in these works will be shown, as well as the highlights of these studies regarding different parameters of importance for the application of AAMs in 3D printing.

Finally, the final considerations present suggestions for studies of interest to the theme, challenges, and differentials of AAMs.

As previously mentioned, AAMs exhibit a significant range of materials that can be part of their composition, leading to diverse results obtained in the variation of parameters that depend on these materials. Furthermore, there is no standard that directs which tests should be carried out for cementitious matrices intended for 3D printing. Thus, this study sought to avoid generalizations, providing information in the most detailed way possible when necessary.

3. Results

3.1. Bibliometric analysis

To evaluate the studies, bibliometric analysis indicators were used, focusing on keywords, study citations, and the countries where these studies are being conducted. The use of these indicators presents researchers in the area with a broad view of the research on the main themes being studied, as well as the visualization of researchers and countries that conduct works related to this approach.

The network maps of this research depict the prevalence of terms through the size of the nodes; larger nodes indicate a higher frequency of a specific term. The connectivity between these terms is highlighted by the formation of clusters, defined based on the co-occurrence of these words in the selected publications. The clusters are presented by distinctive colors for the set of nodes, and their placement varies according to the intensity and frequency of these co-occurrences.

The analysis of keywords was used to quantify the links between them, identify the main research topics, and to which clusters they belong [20].

Table 3 shows the 15 keywords that occurred the most. The total link strength represents the strength of each link; between two keywords, the higher its value, the higher the link. It represents the number of publications in which two terms occur together.

Fig. 3 shows the network map. Analyzing the network map along with the reading of the articles, it becomes evident that when

Table 2
Steps of the review strategy.

Research	**Search: All (titles, keywords, abstracts, introduction)**
	Web of Science (n = 17)
	Scopus (n = 42)
	Duplicate Titles (n = 4)
	Consolidated Basis (n = 55)
Screening and eligibility	**Screening: abstract, introduction, final conclusions, and references**
	Study off Topic (n = 40)
	Consolidated Basis (n = 15)
	Added Manually (n = 44)
	Consolidated Basis Final (n = 59)
Final Analysis	**Full Reading**
	Excluded (n = 4)
	Selected Titles (n = 55)

referring to AAM materials, some articles use variations of the term "Alkali Activated Materials," but in the vast majority, the use of variations of the term "Geopolymers" was identified both on the map and in the written part of the studies, which justifies the emphasis on the map and the strong link with the term "Additive Manufacturing". The map suggests that the most used precursor was fly ash, the most used 3D printing method was extrusion, and the most frequently performed test was the compression test, statements that were proven after reviewing the articles.

Table 4 shows the five most cited articles and their respective number of citations. From the table, one can observe that the citation number is linked to pioneering in the theme. The study by Panda et al. [21] was the second article published on AAMs developed for the 3D application by extrusion with the printing of materials (Available online August 22, 2017). The first was the study by Panda, Paul, and Tan [22](Available online July 27, 2017), but it is a "short communication," in addition to very close publication dates, which justifies the greater number of citations of the article by Panda et al. [21].

Studies on 3D printing with AAMs in the field of civil construction are present in 21 countries. Table 5 shows the ten most active countries in the area, the number of documents developed, the number of citations per country, and the link between these documents in different countries.

Australia presents the Centre for Sustainable Infrastructure and Digital Construction, located at Swinburne University of Technology, in which the institute aims to study environmentally sustainable materials and technologies for the manufacture of civil infrastructure. In Singapore, there is the Singapore Centre for 3D Printing, School of Mechanical and Aerospace Engineering, located at the Nanyang Technological University, which consists of a research center that aims, by various collaborative projects, to insert additive manufacturing in the industry. Both research centers stand out as the affiliation most used in the articles of these countries. China, on the other hand, has six active universities in this area of research among the 13 universities with the most publications, thus it is one of the prominent countries.

In addition, there is a strong interaction between the three countries (Australia, China, and Singapore), as shown in the map of the collaboration network between the countries in Fig. 4. One can identify 6 clusters and greater interaction and activity between Australia, China, and Singapore. The research centers of these countries develop collaborative research aimed at partnerships and are composed of several professors and researchers from other countries. Moreover, by analyzing the articles one can notice that professors from universities in China are part of the research center of Australia and Singapore and vice versa, so that there is a network of collaboration both for the authors and works cited in the article.

3.2. Analysis of 3D printing articles

For a better organization of the results, the analysis of the articles will be presented separately by the printing process: extrusion-based systems and powder-based systems. This division was made because the printing technique is decisive for the mix designs studied and the desired properties.

Extrusion printing can be designed for both off-site and in-site construction. In these applications, mix designs and analyses are made so that the material can be extruded while maintaining its shape after the extrusion process, in addition to supporting the subsequent layers. This method applies to large-scale constructions such as buildings and houses, as well as for producing smaller-scale components [6].

In turn, the powder-based technique is dedicated to off-site construction and allows the manufacture of complex and detailed structures. It is suitable for producing smaller-scale building components that will then be incorporated into on-site construction [27].

In total, 55 studies were analyzed, 48 related to extrusion-based systems and seven related to powder-based systems.

3.2.1. Extrusion-based systems

One of the challenges in applying 3D extrusion printing in construction is determining the mix designs of the printed material since the material must present contrasting characteristics simultaneously. That is, for the layer-by-layer method to succeed without

Table 3
The 15 most used keywords in the studies.

S/N	Keywords	Occurrences	Total Link Strength
1	Additive Manufacturing	44	242
2	Geopolymers	40	232
3	Mechanical Properties	31	192
4	Rheology Properties	29	176
5	Concrete	25	151
6	Fly ash	23	142
7	Waste	21	125
8	Extrusion	14	93
9	Alkali Activated Materials	11	71
10	Cementitious Material	11	74
11	Compression	9	57
12	Cement	8	60
13	Microstructure	7	48
14	Powder Based 3D Printing	6	36
15	Sustainability	6	39

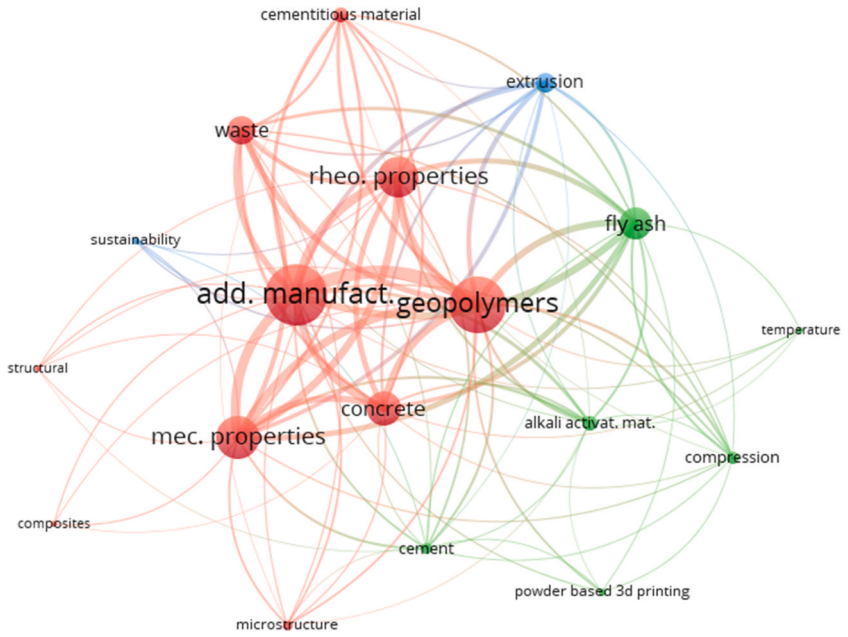

Fig. 3. The network of most used keywords in articles.

Table 4
Ranking of the five most cited studies in the citation network.

	Document	Title	Year of publication	Citations	Links
1	Panda et al. [21]	Additive manufacturing of geopolymer for sustainable built environment	2017	189	17
2	Panda and Tan [23]	Experimental study on mix proportion and fresh properties of fly ash based geopolymer for 3D concrete printing	2018	182	13
3	Panda et al. [24]	Measurement of tensile bond strength of 3D printed geopolymer mortar	2018	179	11
4	Panda, Unluer, and Tan [25]	Investigation of the rheology and strength of geopolymer mixtures for extrusion-based 3D printing	2018	146	13
5	Lim, Panda, and Pham [26]	Improving flexural characteristics of 3D printed geopolymer composites with in-process steel cable reinforcement	2018	90	7

Table 5
Top 10 countries most engaged in AAM research in 3D printing based on studies and citations.

S/N	Country	Documents	Citations	Total Link Strength
1	Australia	15	458	126
2	China	12	374	100
3	Singapore	10	994	168
4	England	5	97	64
5	Germany	4	109	45
6	USA	4	102	28
7	Poland	3	41	42
8	France	2	10	18
9	Italy	2	58	18
10	South Korea	2	26	17

collapse, the material must have fluidity for continuous extrusion without defects. However, after extrusion, the material must maintain its shape even with the increase in pressure from subsequent layer depositions and ensure a bond between these layers [28].

These contrasting characteristics were divided into parameters that are analyzed to assess whether the material is suitable to be applied to 3D printing, that is, has a good “printability”. They are extrudability, shape retention, and buildability.

Extrudability can be defined as the ability of the material to be extruded smoothly without any interruption or obstruction in the flow. Shape retention is the ability of the material to maintain its shape and dimensions after the extrusion process [23]. Buildability is the ability of the material to maintain its shape even with increased stress due to the subsequent layers deposited, without the collapse of the structure [29].

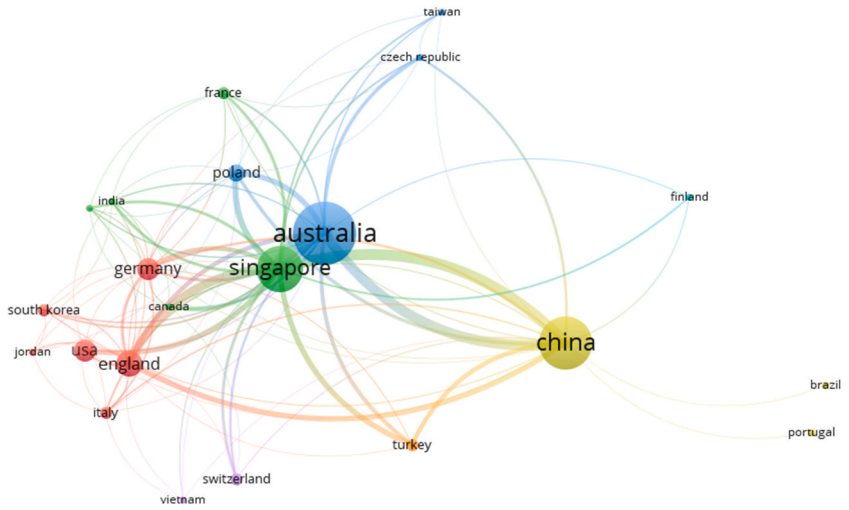

Fig. 4. Network based on the countries of the authors of 55 studies.

3.2.1.1. Materials. In this topic, the materials used in these works will be addressed to show a general overview of the category of AAMs under investigation. Additionally, the influence of precursors, activators, aggregates, additives, and reinforcement on printed AAMs will also be highlighted.

Fig. 5 shows the main precursors used in the studies. The graph illustrates the number of articles that utilized each material as a primary part of the precursor. Furthermore, the tables in Fig. 5 provide information on how these precursors were used, whether as a sole material, combined with other precursors, or combined with materials that by themselves cannot act as precursors but contribute to the formation of the main reaction products.

Reactive silica or alumina-based materials were categorized as additives when incorporated in low percentages (up to 4% to binder).

Although limestone is commonly treated as filler in cementitious composites, alkaline activation studies show that it participates in the structure of polymer gels [30,31], so limestone was considered part of the precursor and not a filler.

Illustration of the Primary Precursors Used and Their Combinations.

Fig. 5 illustrates that the most frequently used precursor is fly ash, particularly Class F, characterized by low calcium content. About 71% of the studies used fly ash, a byproduct of coal-fired thermoelectric plants, as one of the precursors. Fly ash was used as the sole

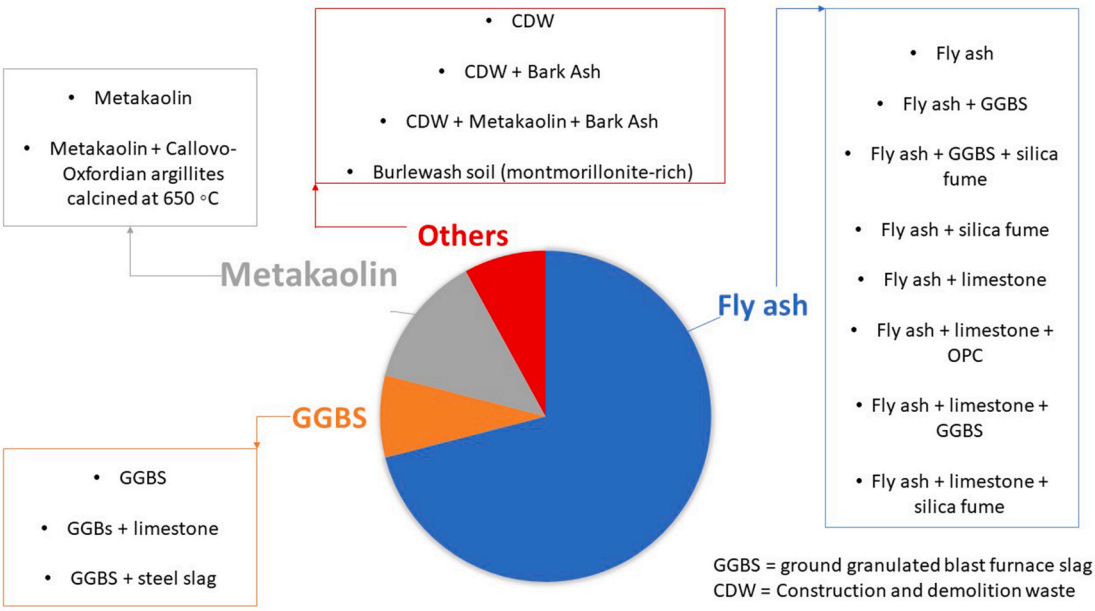

Fig. 5. Illustration of the primary precursors used and their combinations.

main precursor [25,27,32–35] and in different combinations: Fly ash + ground granulated blast furnace slag (GGBS) [25,36–48], Fly ash + GGBS + silica fume [10,21–26,46,49–54], Fly ash + silica fume [25], Fly ash + limestone [55,56], Fly ash + limestone + OPC [55,56], Fly ash + limestone + GGBS [55], Fly ash + limestone + silica fume [56].

On the other hand, GGBS and silica fume primarily served as partial substitutes for fly ash. GGBS was used as a partial replacement at levels up to 50%, while silica fume at levels up to 30%. Only four studies used slag as the main precursor: two of them with GGBS as the sole precursor [57,58], one with limestone [59], and the other with steel slag [60].

Metakaolin was used as a precursor in about 13% of the studies, as the sole main precursor [61–66], with slag [66] and with Callovo-Oxfordian argillites calcined at 650 °C [62]. The other precursors used were Construction and demolition waste (CDW) [67,68], CDW + Bark Ash [69], CDW + Metakaolin + Bark Ash [69], and Burlewash soil (montmorillonite-rich) [70].

The increased use of fly ash as the main precursor is due to different reasons. Firstly, research on AAMs applied to 3D printing has followed trends observed in overall AAM mix design studies. Hasnaoui, Ghorbel, and Wardeh [71] pointed out that out of 125 formulations presented in review articles, 65% were only fly ash-based and, 17% were fly ash with metakaolin or slag.

Another explanation is that, as seen in item 3.1 "Bibliometric analysis," the countries with the highest number of publications on the topic are China and Australia. China was the world's largest coal producer and consumer in 2021 [72] and Australia was the fourth largest producer and 51% of its energy production is derived from coal [72,73]. Other parts of Asia, the European Union, and the USA also occupy places among the five largest consumers of coal in the world ranking [72].

In addition, blast furnace slag and metakaolin may present some challenges regarding their rheology and setting time. Blast furnace slag decreased the setting time when used as a partial replacement for fly ash [23,46,52,53,55]. In addition, when used alone, phase separation can occur during the extrusion process [58,59]. Metakaolin is a material that generally needs a higher water/binder ratio in its mix design, and it can generate a mixture with greater stickness [74].

Fig. 6 shows the activators used and the percentage of studies that used them.

Sodium silicate is the primary activator identified [10,25,27,32–35,38–56,58–61,67–71,75], present in about 75% of the studies; this percentage also includes anhydrous sodium metasilicate powder and grade sodium silicate powder, used in one-part AAMs. Most often, sodium silicate is associated with sodium hydroxide, which is used in about 52% of the studies [10,23,27,32–35,39,45,47,48], [51–54,56,57,59–61,64,67–69,75]. Following sodium silicate and NaOH are KOH [21,36,37,47,48,64,65] and Potassium silicate [21,24,26,36,37,47,48,62], both used in at least one mix design in 15% of the articles. No activator derived from any residue was identified.

About 77% of the studies used some aggregate or filler. Sand, of various origins, was the most used (92% of the studies with incorporation of aggregates/filler and 71% of all the articles) [10,21–27,32–44,46–49,51,52,58,62,66,69,75]; Studies with up to three different particle size distributions of sand were identified, with the largest particle size being 2 mm. Sand/binder ratios were observed in values up to 2.00, but most of the studies used a sand/binder ratio of 1.5 (41% of the studies that presented sand as an aggregate).

The study by Munir, Peltonen, and Kärki [69] used mine tailings sand in their research, while Ilcan et al. [68] used recycled concrete as aggregate and Valente et al. [51] studied the replacement of sand with Ground waste tire rubber (GWTR).

The additives traditionally used in civil construction are produced for their application in matrices with Portland cement, thus it is of great interest to identify the additives applied to AAMs and understand their respective roles. For example, sucrose and borax are applied as retardants, while cellulose-based additives (CMC, HPMC, and HEC) are viscosity-modifying agents. Magnesium aluminum silicate and attapulgite are thixotropic enhancers; such additives are similar, but for lack of greater details the authors of this study preferred to keep them in distinct categories. Hydromagnesite was employed to promote nucleation. Table 6 shows the additives identified in the studies and the respective articles in which they were used.

About 40% of the authors studied the application of reinforced AAMs in 3D printing since the material can be considered brittle. Incorporations of up to 6% reinforcement were observed, but most authors studied incorporations in lower levels, up to 1%.

Most authors studied reinforcements with randomly distributed fibers, but some authors studied reinforcements with continuous cables [10,26,49]. Table 7 displays the fiber reinforcement identified in the studies and the corresponding articles where they were

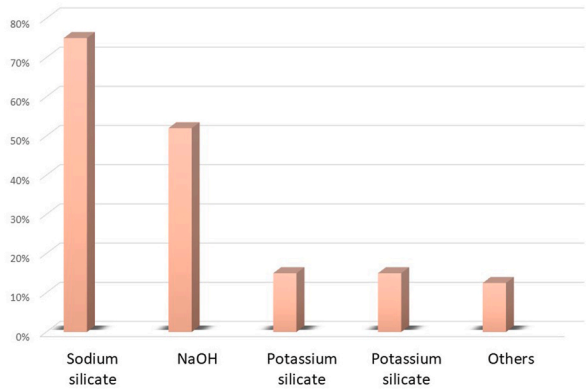

Fig. 6. Graph showing the activators used and the percentage of studies that used each one. Among the "others" are included: CsOH [64], Sol-silica [64,65], Sodium sulfate and $Ca(OH)_2$ (In combination with NaOH and/or sodium silicate) [67,68].

Table 6
Additives used in the reviewed articles.

Additives	Reference
Alumina powder	[55]
Sodium carboxymethyl starch (CMS)	[57,59]
Surfactant	[64,65]
Sucrose powder	[38,40,43,48]
Magnesium Alumino Silicate (MAS)	[26,43,46]
Sodium carboxymethyl cellulose (CMC)	[47,48,75]
Attapulgite clay	[23,36,54,58]
Borax	[42,47,48]
Hydroxypropyl methylcellulose (HPMC)	[22]
Surfactant	[56]
Hydromagnesite seeds	[58]
Superplasticizer	[60,66]
Redispersible latex	[60]
Defoamer	[60]
Hydroxyethyl cellulose (HEC)	[10]
Kaolin (up to 4% of incorporation in relation to binder)	[62]
Nano clay (no specification)	[40,48]
Comercial VMA	[66]

utilized.

3.2.1.2. Influence of precursors on the 3D printed AAM. This topic highlights the results obtained regarding the influence of the type of precursor in composites. Since the chemical composition and morphology of the material affect its behavior in the fresh and hardened state.

As mentioned in item 3.2.1.1, fly ash is the main precursor in 71% of the studies, but the incorporation of other materials as part of the binder, such as GGBS, OPC, and silica fume were also studied.

Concerning GGBS, its rapid reaction and particle morphology influenced the setting time, open time, rheology, flowability, and mechanical behavior of AAMs. Table 8 compiles the results showing this time difference between AAMs with different percentages of fly ash replaced by GGBS.

This phenomenon is associated with an increased presence of Ca^{+} ions with the incorporation of slag, leading to the rapid formation of C–S–H gels. Kumar, Kumar, and Mehrota [76] performed a calorimetry test with different fly ash to slag replacement contents (GGBS). It was observed that the peaks generated are typical of the dissolution precipitation reaction leading to the formation of C–S–H. In addition to this, there was a significant increase in the peak with the increase in slag content, as well as more left-shifted peaks, that is, the faster appearance of the peaks.

The replacement of fly ash by GGBS leads to an acceleration of geopolymerization, which also influences the rheological behavior of the mixtures. Panda, Unluer and Tan [25] analyzed the evolution of the yield stress for different mix designs of fly ash based AAMs, activated with sodium hydroxide and silicate. The mix design with only fly ash (F100) obtained the lowest yield point for all times, and from 10 min onwards, the yield point for mix designs with the presence of GGBS (5 and 10%) grew exponentially. This same phenomenon was observed in thixotropic behavior regarding time.

Guo, Yang, and Xiong [46] reported that the replacement of fly ash by GGBS, in the contents of 10 and 20%, generated an increase in plastic viscosity and improved thixotropy in AAMs activated with anhydrous sodium silicate. A reasonable plastic viscosity can mean that the material is pumpable without running the risk of segregation, while a good thixotropy can represent the stability of the

Table 7
Types of reinforcement used in the reviewed articles.

Reinforcement	Reference
Carbon fiber	[32,34,65,69]
Polypropylene fiber (PP)	[10,27,33,66,75]
Polyvinyl alcohol fiber (PVA)	[26,27,44,48,54]
Polyphenylene benzisoxazole fiber (PBO)	[27]
Glass fiber	[22,23,61,62]
Micro steel cable	[10,26,49]
Flax fiber	[32,34]
Micro nylon cable	[49]
Micro aramid cable	[49]
Micro polyethylene cable (PE)	[49]
Micro carbon cable	[49]
Steel fiber	[33]
Glass wool	[69]
Wollastonite needles	[62,63]
Nano-graphite platelets	[52]

Table 8
Results showing the influence of replacing fly ash with GGBS concerning setting time/open time.

GGBS content (%)	Other precursors	Activators	Initial and final setting time (minutes)	Open time (minutes)	Reference
0%	Fly ash	Anhydrous sodium silicate	151–228	–	[46]
10%			50–71		
20%			28–37		
30%			18–30		
15%	Fly ash +	Sodium silicate and sodium	47 (initial)	35	[53]
25%	Silica fume	hydroxide	35 (initial)	20	
35%			12 (initial)	10	
0%	Fly ash + Limestone	Sodium hydroxide	~270 (initial)		[55]
30%			90 (initial)		

material to its weight and even with the addition of the subsequent layers. However, high slag values (30%) can impair rheology, that is, cause a drop in plastic viscosity and thixotropy, compared to lower slag contents.

Panda et al. [37] observed an increase in apparent viscosity, static yield stress, thixotropy, and compressive strength with increasing replacement of fly ash by GGBS for "one-part" geopolymers activated by potassium silicate and potassium hydroxide.

In casted samples, several studies demonstrate the mechanical benefits of replacing fly ash with GGBS. However, when applied to 3D printing, these benefits are entirely subject to the rheological conditions of the printed AAM. For example, in the study conducted by Albar et al. [53], the superior mechanical performance of the printed samples wasn't related to the GGBS content but rather to the dosage that retained the best shape.

Blast furnace slag has an angular particle, which generates an interlocking effect between the particles and may decrease the fluidity of the AAMs, while fly ash has spherical particles, which generate a rolling effect and possible improvement in flowability. Chougan et al. [52] reported that reducing the slag content and increasing the other precursors (fly ash and silica fume) contributed significantly to the increase in fluidity. The most fluid dosage was the one with the highest percentage of fly ash, as its spherical particle shape generated a rolling effect.

The majority of studies on fly ash substitution have been dedicated to GGBS. However, it's important to note some observations regarding other components of the precursor that could be interesting for 3D application.

Regarding the influence of OPC in the mixtures, this material also accelerated the reactions, considerably reducing the setting time, although not as much as GGBS. The OPC increased the yield stress and apparent viscosity of the mixture, more than the slag. This was attributed to its smaller particle diameter. Additionally, the effects of particle shape and surface charges of Portland cement, influencing flocculation, might have contributed to this behavior [55].

The fine particles of silica fume and its large surface area enhance the packing of dosages and increase flocculation when used as a partial replacement for fly ash in AAMs. Consequently, mixtures with the presence of silica fume exhibited an increase in apparent viscosity [46], thixotropy [25,46], and yield stress [25,46]. Concerning the setting time, silica fume did not have a great influence on this property [46].

Regarding unconventional precursors, bark boiler ash with contents higher than 10%, activated with sodium silicate, presented a high water demand, absorbing the liquid before mixing with the other materials, so the maximum indicated content is 7% [69]. The precursors derived from construction and demolition waste showed very low mechanical performance for contents above 27% [69]. It is important to emphasize that to achieve a mixture with higher compressive strengths, it was necessary to include metakaolin as part of the precursors for both bark boiler ash and demolition waste.

Pasupathy, Ramakrishnan, and Sanjayan [40] analyzed the replacement of fly ash by brick waste in one-part AAMs at levels of 10, 20, and 50% in relation to precursors (FA + GGBS). The higher water demand of brick waste and its irregular shape caused a decrease in the diameter in the flowability test of 3.3, 7.9, and 11.5% as the incorporation content increased. The lower reactivity of brick waste increased the initial setting time by up to 23 min but caused a decrease in compressive strength for replacement contents greater than 10%; the decrease in strength varied according to the type of cure, between casted and printed samples and for the latter, depending on the direction of loading in relation to the printing path. Interlayer bond strength followed the same trend as the compressive strength results. The results of compressive strength and interlayer bond strength are related to the apparent porosity of the samples.

3.2.1.3. Influence of activators on the 3D printed AAM. In general, regardless of the type of AAM system, the reaction begins with different dissolution steps, releasing Al, Si, and Ca (when present) in the solution, which will react and reorient to form binding products. The reaction products then evolve into a more developed and complex microstructure, becoming a hardened product [77].

Different parameters influence the speed of this process and the products formed; for example, the type and concentration of the activator, precursor type, and SiO_2/Na_2O ratio, in addition to the type of cure.

The most commonly used activators are sodium or potassium derivatives. However, these cations (Na^+ and K^+) have a difference concerning their size, with the K+ion (1.33 Å) being greater than Na^+ (0.97 Å), which leads to a physical, chemical, and hydration difference in the forming structure [78].

Bong et al. [47] and Bong et al. [48] reported that for AAMs based on fly ash and GGBS (3:1), mixtures based on potassium hydroxide and silicate as activator presented shorter open times, smaller opening diameter in workability tests, and lower values of compressive strengths after 3 days of ambient curing compared to mixtures activated with sodium hydroxide and silicate.

The influence of these different cations has been shown to be different in the literature for GGBS and fly ash. Regarding GGBS, in the study by Tänzer, Jin, and Stephan [79], the initial setting time for the potassium-based mix designs was significantly lower than for the sodium-based activated AAMs. Concerning compressive strength, mix designs with potassium-based activators reached higher strength values than mix designs with sodium-based activators with the same SiO_2/M_2O ratio for the two types of GGBS studied.

Regarding the fly ash-based AAMs, Król et al. [80] used the attenuated total reflectance-Fourier transform IR (ATR/FT-IR) technique to evaluate the geopolymerization process of fly ash-based AAMs activated with NaOH and KOH. The authors reported that both presented a similar activation process, but when activated by KOH the phase related to condensation and reorganization of the aluminosilicate gel occurs much more slowly, that is, the kinetics of geopolymerization with potassium-based activator occurred more slowly than for the sodium-based activator, for fly ash as a precursor.

Thus, based on the studies of Tänzer, Jin, and Stephan [79] and Król et al. [80], it is believed that the shortest open time for potassium-activated AAMs in the study by Bong et al. [47] was due to the presence of GGBS. As seen in item 3.2.1.1.1, GGBS coordinates the setting time of AAMs composed of fly ash and GGBS, and, when the AAM is activated by potassium, it causes its setting time to be shorter than when activated with sodium [79].

Sitarz et al. [81] analyzed the compressive strength of AAMs activated with sodium and potassium silicate, varying the replacement content of fly ash by GGBS in 10, 30, and 50%. At 3 days of curing, the compressive strengths obtained for potassium-based AAMs were similar to or lower than the sodium-activated AAMs. Nevertheless, at 28 days, except for the mix design with 10% GGBS, the strengths with potassium-based activators were higher. The authors associated this increase in the values of the initial strengths of sodium-activated AAMs with the smaller size of the Na^+ cation, which leaves it with greater mobility in the matrix, causing the activator to release more silicate and aluminate monomers. For systems with only GGBS, the mix designs activated with potassium reach higher strength values at 7 and 28 days [79]. Thus, the reduced compressive strength values of AAMs reported in the study by Bong et al. [48], utilizing a potassium-based activator, are attributed to the interaction between activators and the higher quantity of fly ash present, as well as the relatively shorter curing time of the samples (3 days).

The concentration and ratios of AAM activators are crucial parameters for the application of AAMs in 3D printing. Table 9 compiles the results from studies that varied the activator and the corresponding outcomes resulting from this variation.

Referring to Tables 9 and in the study by Muthukrishnan, Ramakrishnan, and Sanjayan [39], the yield strength evolution, measured by the penetrometer, notably increases with rising SiO_2/Na_2O ratios, except for 0.54. The authors justified this exception by the predominance of C–S–H gels over steric repulsion by silicate anions. That is, for silicate-activated slag-based AAMs, the silicate anions reduce inter-particle attraction in the dissolution phase due to a combined effect of electrostatic repulsion and steric hindrance. However, after a certain silicate content, the attraction between particles, due to the formation of C–S–H gels, increases and overcomes the repulsion, which results in faster evolution of the yield point. Conversely, the dynamic yield strength assessed by a rotational rheometer at time zero declined with increasing SiO_2/Na_2O ratios. This was linked to increased shear-thinning from higher silicate content, benefiting from the repulsive behavior of silicate anions. However, at elevated silicate values, the swift development of C–S–H countered this repulsion force, which explains the similar slump values (12.7 mm) and scattering diameters (6.3 mm) for SiO_2/Na_2O mix designs of 0.34 and 2.15.

However, in the work of Zhang et al. [60], there was an increase in yield stress as the Si/Na ratio decreased, which was attributed to the acceleration of the dissolution of aluminosilicates by the higher presence of Na^+. Decreasing this ratio also increased the ability of structural rebuilding. Both studies indicated an increase in compressive strength as the Si/Na ratio increased.

For one-part AAMs [37], the increase in the static yield stress, as the percentage of activator increased from 10 to 20%, was

Table 9
Results obtained by varying the activators in different tests.

Precursors	Activators	Variable	Outcomes			Reference
Fly ash and GGBS (1:1)	Sodium silicate and NaOH	SiO_2/Na_2O	Yield strength (kPa)	Dynamic yield strength (Pa)	Compressive strength (MPa) 7 and 28 days	[39]
		0.34	91.00	520	~12–14	
		0.54	54.60	180	~15–25	
		1.04	99.20	110	~14–52	
		1.17	326.70	Not able to measure	~44–59	
		2.15	467.7		~49–62	
90% GGBS and 10% Steel slag	Sodium silicate and NaOH	SiO_2/Na_2O	Yield stress (Pa)	SRE[a] (J/s^am^2) 1 and 20 min	Compressive strength (MPa) 7 days	[60]
		1.0	0.339	~71–114	48.39	
		0.9	0.679	~75–123	53.04	
		0.8	1.549	~88–127	49.04	
		0.7	1.824	~92–128	46.61	
		0.6	2.080	~102–138	40.26	
		0.5	3.439	~104–140	37.90	
70% fly ash and 30% GGBS (One-part)	Potassium silicate and KOH	Percentage of the precursor's mass	Apparent viscosity (Pa.s)	Static yield stress (Pa)	thixotropic parameter (λ)	Compressive strength (MPa) 7 days	[37]
		10%	7.20	3400	1.09	~25	
		15%	7.60	3400	1.50	~17.5	
		20%	8.00	4200	1.27	~44	

[a] Specific rebuilding energy.

associated with a higher pH and ionic strength of the surface charges. The improvement of the compressive strength, between 10 and 20%, was attributed to the higher presence of Si ions available for geopolymerization, but the mix design with 15% reached the value of 17.5 MPa. Concerning thixotropy, the authors attribute the decrease in thixotropy for the 20% mix design to weaker bonds between the colloidal particles due to the effect of silicate, which could be adsorbed on the surface of the particles, increasing the distance between particles.

For CDW-based geopolymer mixtures, Şahin et al. [67] varied the molarity between 5 and 15 M with additions of 1.25 M, and, for each molality value, they varied the incorporation of $Ca(OH)_2$ in percentages of 0, 2, 4, 6, 8, and 10% in relation to the precursor, for a w/b fixed at 0.33. For all molality values, there was an increase in buildability and a decrease in flowability as the $Ca(OH)_2$ content increased. In the compressive strength test at 7 and 28 days, in addition to the variation of molality and $Ca(OH)_2$ content, the variation of the Na_2SiO_3/NaOH ratios of 0, 0.5, and 1 were also added. In general, samples with $Ca(OH)_2$ presented higher compressive strengths, especially after 28 days of curing, but the optimal $Ca(OH)_2$ content varied according to the molality and Na_2SiO_3/NaOH ratio.

Ilcan et al. [68] also noted this behavior regarding flowability and buildability for CDW-based AAMs, with different molarities of NaOH (7.5, 10, 12.5, and 15 M) and different incorporation contents of $Ca(OH)_2$ (0, 4, 8, and 12%) to precursor mass. The incorporation of $Ca(OH)_2$ did not significantly alter the open time of the mixtures.

The use of NaOH as an activator for the CDW-based mixtures presents a "turning point," that is, for values below 10 M, as the increase in molarity occurs (7.5–10 M), there is an increase in the flow index and decrease in buildability. After the value of 10 M, as the increase in molarity occurs (12.5–15 M), there is a drop in the flow index and an increase in buildability [68]. The increase in flowability up to 10 M was attributed to the higher dissolution rates of the precursors under greater alkalinity and the imbalanced surface charge affected by Na^+ ions. This imbalance can create more repulsive forces and result in lower yield stress. However, the drop in flowability after 10 M was explained by the increased Na + concentrations within the matrix as the NaOH molarity increased. Beyond 10 M, the surface of precursors is charged with more positive charges, and repulsive forces induced by the negative charges on the surface of precursors decrease. Consequently, the geopolymer matrices exhibited higher yield stress. Additionally, the higher molarity led to a significant increase in ionic species, restricting ion mobility, which further contributed to the decreased flowability.

3.2.1.4. Influence of aggregates/fillers on the 3D printed AAM. Something important to highlight in this topic is the contrast between economy and printability for AAMs in 3D printing. Higher aggregate contents can reduce costs, but they may also lead to clogging issues and even the addition of water cannot solve this problem; this phenomenon is due to the effect of interlocking and friction between particles, hindering the flow [23]. Panda and Tan [23] observed this clogging effect for sand/binder ratios of 1.7 and 1.9.

Regarding the particle size distribution of aggregates, Chougan et al. [52] compared two mixtures with differing granulometric values of sand for AAMs containing 60% fly ash, 25% GGBS, and 15% silica fume. The first mix design comprised 60% sand particles ranging from 0.5 to 1 mm and 40% from 0 to 0.5 mm, whereas the second mixture consisted of 40% of sand particles between 0.5 and 1 mm and 60% between 0 and 0.5 mm. The increase in finer sand particles in the second mixture resulted in a greater surface area of the aggregates, subsequently elevating their yield shear stress and plastic viscosity (i.e., 18.58 Pa and 11.03 Pa s) compared to the first mixture (13.43 Pa and 6.82 Pa s). This also led to better shape retention of the blend with finer sand during the printing process. However, the setting time and open time were not affected by the variation in sand particle size distribution.

Valente et al. [51] investigated the substitution of sand with Ground Waste Tire Rubber (GWTR) in AAMs comprising fly ash, GGBS, and silica fume, exploring replacement ratios of 50% and 100%. They considered two GWTR granulometries: rubber powder (RP) with a nominal size gradation of 0–1 mm and rubber coarse (RC) sized 0–3 mm. The introduction of GWTR, irrespective of RP or RC content, notably reduced flowability, restricting printing to nozzle diameters of only 20 mm instead of 10 or 15 mm. The hydrophilic nature of rubber led to weak and porous interfacial transition zones, degrading the mechanical properties of both printed and casted AAMs. However, the primary aim of utilizing this waste was to produce lightweight concretes with a unit weight below 1800 kg/m^3, successfully achieved across all rubber-containing mix designs. Moreover, replacing sand with various GWTR granulometries resulted in reduced thermal conductivity. Additionally, acoustic insulation improved within the low to medium frequency range, showing enhancements of at least 90%.

3.2.1.5. Influence of additives on the 3D printed AAM. Different additives are used to modify the properties of cementitious matrices. However, when used in alkali-activated matrices, their effects may be diminished or hindered due to high alkalinity or a lack of affinity with the system. In additive manufacturing, the incorporation of additives significantly contributes to achieving the necessary rheological properties. Hence, the study of the effects of traditional additives on AAMs and the search for additives that are compatible with them are of great importance. Researchers have focused on studying the impacts of various additives, which will be discussed in this topic.

CMS is a rheological modifier derived from the starch etherification reaction. The hydroxyl and/or carboline groups present in the material can bond with water molecules by hydrogen bonding, promoting an increase in viscosity [57]. Attapulgite clay is a thixotropic material, due to its positive and negative charges; during the flow, the particles align in the direction of the flow due to the repulsion of similar charges, but when the material is at rest, the opposite charges attract and flocculate to form a colloidal network [36].

Hydromagnesite serves as a nucleation seed to enhance mechanical and rheological properties. Magnesium aluminum silicate (MAS) functions as a thixotropy promoter, inducing flocculation through electrostatic interactions and exhibiting a filler effect owing to its dipolar surface and particle morphology [43].

Fig. 7 displays the studied additives and their influence on the properties of AAMs. It's important to highlight that despite these

observed results, the action of additives may vary depending on the materials (precursors and activators) and proportions used.

Sun et al. [59] reported that during the printing process, there was a phenomenon of segregation and collapse of the mixtures for the mix designs based on GGBS and calcium carbonate (1:1), activated with sodium silicate and hydroxide and with CMS in the contents of 0 and 2%; in turn, the mix design with 8% of CMS presented discontinuity due to its high yield stress and plastic viscosity, but it was possible to make the extrusion of the AAMs with CMS contents of 4 and 6% without collapse and discontinuities.

Chougan et al. [54] noted that for AAMs composed of fly ash (60%), GGBS (25%), and silica fume (15%) and activated with sodium silicate and hydroxide based, the incorporation of 0.5% attapulgite clay decreased the flowability of the mixture, obtaining a flowability of 18% after 5 min; the mix design with 1% of clay obtained flowability of 25%, and the worsening of flowability was attributed to the high water absorption by the additive, which presents fine particle size and high specific surface; the worst flowability for the mix design with 0.5% compared to 1% was explained by the greater separation of the additive particles, decreasing flowability. It was not possible to perform the shape retention test for the sample with 0.5%, since it was not printable, but the mix design with 1% was printable, which might indicate that the influence of additives on AAMs doesn't necessarily follow a linear pattern.

In this study developed by Muthukrishnan, Ramakrishnan and Sanjayan [43], it was possible to print an AAM with 0.75% magnesium aluminum silicate and 1.5% sucrose with more than 120 layers (>1.4 m) without collapsing, showing that the combination of different additives can also result in a successful print (Fig. 8).

Alghamdi and Neithalath [56] studied AAMs printed with thermal efficiency due to porosity. To obtain this porosity, a surfactant was used as a foaming agent and foam stabilizer. The printed geopolymers with foam obtained low values of thermal conductivity (between 0.15 and 0.3 W/m-K), but they are higher values than the conventional materials used (less than 0.05 W/m-K). Thus, the authors proposed a precast sandwich concrete panel composed of two layers of concrete separated by a printed geopolymeric with suitable architecture. Its properties and geometry were changed according to the requirements of the construction, following the analytical model effective media theory (EMT) for an air volume fraction between 60 and 70%; the EMT predicts that the thermal conductivity will be similar to commercial insulation products.

3.2.1.6. Influence of the use of reinforcement on the 3D printed AAM. The randomly distributed fibers are applied in 3D printing due to their ease of application in the mixture and their action on the tensile and flexural performance of composites, especially after the beginning of cracking, since they create bridges between the cracks, allowing the transfer of stresses.

Different studies have observed an improvement in flexural performance by adding randomly distributed fibers. Nematollahi et al. [27] studied the incorporation of different types of polymeric fibers (PVA, PBO, and PP) in AAMs based on fly ash, activated with NaOH and sodium silicate. The fibers were incorporated in a volume fraction of 0.25%. The fiber-free composite obtained a flexural strength of 7.7 MPa, while the reinforced composites obtained values of 9 MPa (PP), 9.5 MPa (PVA), and 10.3 MPa (PBO).

In the study by Ma et al. [65], carbon fiber improved the flexural and compressive strength performance of metakaolin-based AAMs, but it was observed in the load-displacement curve that the composites maintained brittle failure mode. Short carbon fibers were incorporated in percentages of 0, 1, 2, 3, 4, 5, and 6%, and the optimal incorporation value established was 3%.

The use of nano-graphite platelets (NGPs) also improved flexural strength for fly ash, GGBS, and silica fume-based printed

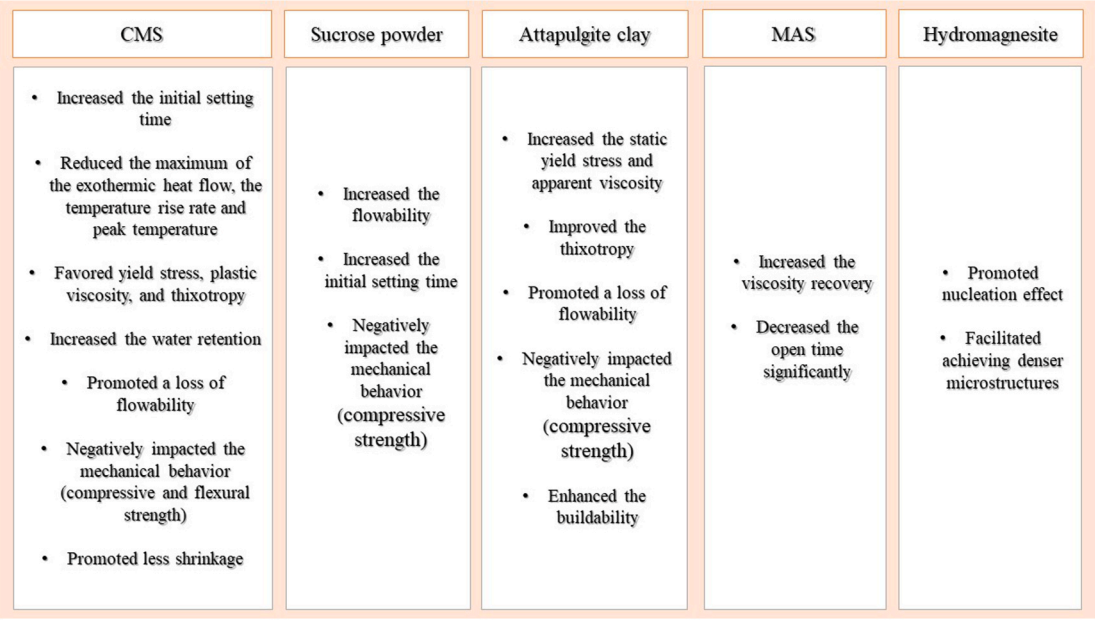

Fig. 7. -Studied additives and their influence on AAMs: CMS [57,59]; sucrose powder [38]; attapulgite clay [36,54]; MAS [43] and hydromagnesite [58].

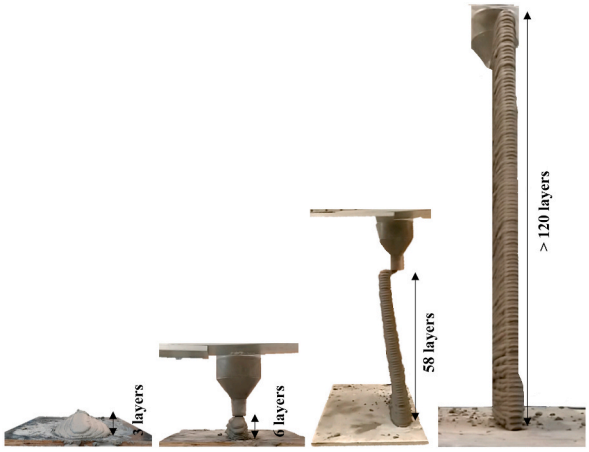

Fig. 8. Printed structures: the last one, comprising more than 120 layers, was printed using a combination of magnesium aluminum silicate and sucrose [43].

composites, activated with sodium silicate and hydroxide. The incorporation of 1% of the reinforcement in the printed composite, to the mass of the AAM, increased the flexural strength from 8 MPa, without fibers, to 15.3 MPa [52].

The incorporation of PP fibers in volumes of 0.25, 0.5, 0.75, and 1% did not show a significant improvement in flexural strength in

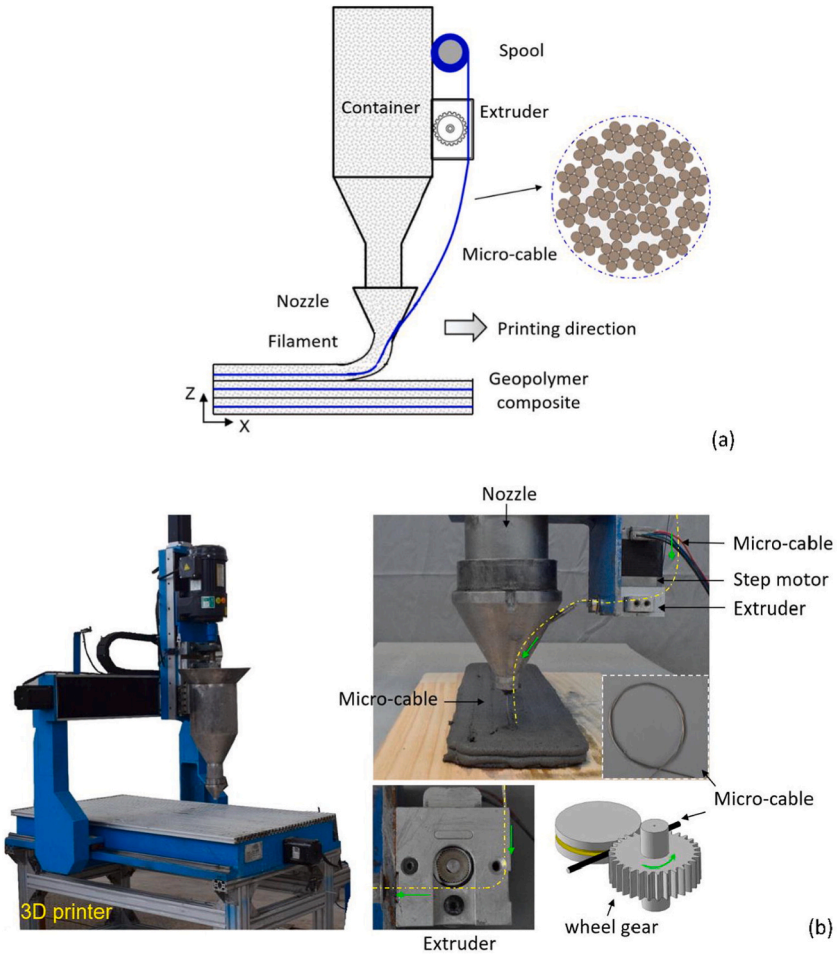

Fig. 9. (a) Schematic illustration and (b) Set-up of 3D printer and entertaining process of micro-cable into geopolymer filaments [10].

the study by Nematollahi et al. [75]. Despite the inexpressive effect on flexural strength, the failure mode was changed to values above 0.25% of fiber incorporation, by the curves of flexural stress vs. mid-span deflection, it was possible to observe a change from brittle to ductile.

In terms of using unconventional materials and valorization of by-products, Korniejenko, Kejzlar, and Louda [32] compared the incorporation of 1% carbon fiber (by mass of composites) with the fiber of green tow flax, a by-product of textile fiber production, in fly ash-based AAMs and activated with NaOH and sodium silicate. The composites were produced by injection process, simulating 3D printing, and after 28 days of curing, the composites with carbon fiber presented lower compressive and flexural strength values (38.7 and 8.1, respectively), while the composites with flax fibers presented values of 48.7 and 9.4 MPa. The authors indicated that the better mechanical behavior may be due to better cohesion between the fiber and the matrix, observed in the SEM test.

Regarding the influence of randomly distributed fibers on printing capacity properties, improvements were observed concerning shape retention capacity [52,54,75]. Nevertheless, the increase in the stiffness of the fresh mixture that causes this better retention in the shape can impair the bond between layers since it decreases the deformation capacity of the layer and the formation of a unified interface and reduces the homogeneity of the composites, as it is difficult to control its distribution, which can lead to irregular surfaces, which also contributes to a worse adhesion between layers [27,33] and accentuates the anisotropic behavior of the printed samples [75].

In addition to the use of distributed fibers, there is the possibility of inserting continuous micro-cables, simultaneously with the printing process. Fig. 9 (a) and (b) [10] illustrate how the insertion of this micro-cable works.

Fig. 10 (a) and (b) depict the nozzle developed by Lim, Panda, and Pham [26] to enable the simultaneous insertion of micro-cables along with the extrusion of the matrix.

In the study by Lim, Panda, and Pham [26], the behavior of a composite with short-fibers (PVA) only was compared with a composite with hybrid reinforcement (PVA and steel cable). The AAMs were produced with fly ash, GGBS, and silica fume, activated with potassium silicate, and incorporated 0.5 wt % of 8 mm PVA fiber. The use of hybrid reinforcement brought an improvement in the mechanical behavior in the four-point bending test. This shows the good interaction between short-fiber and micro-cable since the cable was responsible for most of the tensile strength after crack; however, as the elongation of the micro-cable occurred, secondary cracks caused by the cable pull-out appeared, but the PVA short fibers restricted these small cracks.

Ma et al. [10] reinforced AAMs composed of fly ash, GGBS, and silica fume with a 1.2 mm diameter continuous stainless steel micro-cable. The composites were printed with three different printing paths (A, B, and C) and compared with a composite with only 0.56% PP fibers. The composites with the micro cable obtained flexural strength higher than the composite without cable, regardless of the printing path, but there was a variation in the results for the three paths. The composites with continuous reinforcement reached ultimate deflection significantly higher than the composite with only PP fiber.

3.2.1.7. Methodology. This section outlines the methodologies employed by the authors of the reviewed articles to assess various properties. In this topic, the influence of printing parameters and temperature on printed AAMs will be discussed, along with the properties of these printed AAMs compared to casted ones. Additionally, correlations between analyses and printing properties will be explored.

Table 10 illustrates the analyses conducted to evaluate the mixtures in their fresh state.

Some studies used parameters obtained in different tests (e.g. rheometry, slump test, among others) to indirectly evaluate the printing properties (buildability, shape retention, and extrudability). However, for better organization, the authors divided the methods into indirect and direct in Tables 10 and 11. That is, indirect methods have been assigned to what they determine, not what they are associated with.

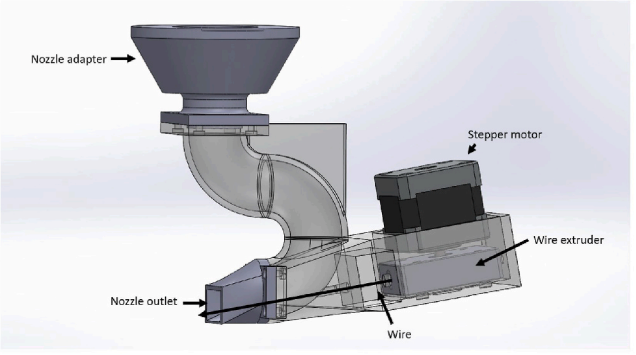

(a) Schematic of the nozzle equipped with the cable extruder system.

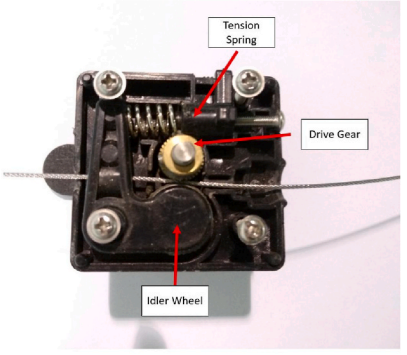

(b) Top view of the cable extruder prototype.

Fig. 10. (a) Schematic illustration of the design and (b) Prototype of the steel cable extruder developed at by Lim, Panda, and Pham [26] Nanyang Technological University (NTU).

Table 10
Methodologies used in the analyzed studies – Fresh state.

Analyses conducted	References
Rheometry	[21,23–25,35–40,43,44,46,48],[50,52–54,56,57,59,61,64–66,70]
Determination of setting time	[36,38–40,50,52,53,55,57,59,61,63,69]
Isothermal calorimetry	[25,36,43,57]
Flowability/workability analysis	[33,38,40,42,48,51–55,59,67–69,75]
Extrudability analysis	[23,38,42,48,51,55,58,68]
Shape retention capacity analysis	[23,36,40,42,47,48,52,53,56]
Buildability analysis	[23,37,38,42,43,48,51,52,54,55,58,66,67]
Determination of open time	[42,47,52–54,69]
Load carrying capacity	[21,23,37,39,67,75]
Ram extrusion tests	[55,67]
Accuracy of the 3D printed products	[62,64]
Fourier-transform Infrared Spectroscopy (FTIR)	[39,43,44,57]
Adsorption measurement of the additive in the precursor	[57]
Measures of the zeta potential of pastes	[57]
Matrix densification analysis	[39]
Analysis of foam expansion	[56]
Determination of moisture content on the surface	[44]
Temperature setting tests	[69]
Vane shear test	[67,68]
Analysis of paste temperature evolution	[57]
Mixturability analysis	[69]
Analysis of water retention capacity	[59]

It is also important to mention that some studies related the results obtained in the indirect methods with the results obtained in the direct methods.

Rheometry is included in 54% of the studies (Table 10), being the most used evaluation for analyzing mix designs in the fresh state. It is followed by the determination of setting time and flowability/workability analyses. Rheometry was mostly performed to determine the yield stress of the mixtures, their apparent viscosity, viscosity recovery capacity, and study of thixotropy, among others.

Upon analysis of the methodologies employed in the articles, a significant variability in chosen tests among researchers was observed. Additionally, the execution of these tests displayed considerable diversity. Notably, there were disparate recommendations for analyzing properties such as buildability, shape retention, interlayer bond, and others. This variability stems from the absence of standardized norms guiding researchers on which analyses to conduct and the specifications for each. Consequently, the authors resorted to employing tests established in standards for alternate applications or modified tests derived from previous publications.

Table 11
Methodologies used in the analyzed studies – Hardened state.

Analyses conducted	References
Compressive strength test	[21,22,24,32,34,36–40,42,43,47–56,59,60,64,65,67–70,75]
Flexural test	[10,21,22,24,26,27,32–34,38,43,48,51–55,59,62,65,69,75]
X-ray diffractometry (XRD)	[21,32,37,58,59]
Microscopic Analysis	[21,26,32,36,37,40,41,46,52,54,56,58,59,62,64,65,70]
Evaluation of drying shrinkage	[59]
Pull-out test	[49]
Computer simulation	[64,65]
Determination of bulk density	[21,24,34,38,40,52,53,64]
Evaluation of adhesion between layers	[21,24,27,40,44,48,75]
Determination of modulus of elasticity	[64]
Determination of Poisson's coefficient	[64]
Determination of apparent porosity	[38,40,64,75]
Mercury Intrusion Porosimetry (MIP)	[55,56]
2D evaluation of voids	[54]
Micro X-ray tomography	[35,54]
Tensile test	[22,24,48,49]
Evaluation of reinforcement/matrix adhesion	[50]
Determination of the specific mass of composites	[56]
Analysis of thermal conductivity of composites	[51,56]
Evaluation of stiffness	[44]
Evaluation of lateral deformation	[44]
Determination of moisture content on the surface	[44]
Determination of moisture loss	[44]
Shear performance evaluation	[49]
Determination of the unit weight	[51]
Dynamic mechanical thermo-analysis (DMTA)	[51]
Acoustic insulation analysis	[51]

The type of cure can influence the reaction of AAMs and, consequently, their mechanical behavior. For the studies directed to its application in 3D printing, 59% of the authors opted for ambient curing [21,24–26,36–38,42,44,46–50,55,59,62,63,68], with or without moisture control, which is consistent with the desired on-site application in extrusion 3D printing. The other mix designs were cured thermally and at room temperature [27,32–34,40,48,51–54,75], only thermally [56] and in immersion [39,43].

Table 11 outlines the analyses used to characterize the AAMs in their hardened state.

About 67% of the authors included the evaluation of compressive strength in their work (Table 11), followed by the flexural test, included in about 46% of the studies. However, there is also variability in what is being evaluated. Some authors performed these tests with samples extracted from a filament printed with one or more layers; other authors printed the samples with only one filament; and others chose to perform these tests with samples casted in the traditional way of testing.

The articles analyzed followed the trend of mechanical characterization of traditionally casted mortars/concretes, with the compressive strength test also being the most used. The main objectives of the mechanical tests in these studies were to compare differences between mix designs, verify whether there is a mechanical difference by varying the orientation of the loading in relation to the sample, compare the difference in performance between printed and casted samples, study the influence of the bond between layers on mechanical behavior, that is, they were used as a comparison metric and not classification since there is no governing standard to classify composites and designate them to a niche of application.

Regarding 3D printing technology, the most used type of printer is the gantry printer [10,22–26,36–40,42,43,46,48–50,52–60,66–68], followed by robotic arms [21,63,70]. In the methodologies implemented in the construction industry there is also this trend: out of 13 techniques employed by material extrusion, eight use the gantry system (Contour Crafting, 3D Concrete Printing, Winsun, Total Kustom, Vulcan II, BOD2, and HuaShang Tengda), three use robotic arms (Apis Cor, XtreeE, and CyBe RC 3Dp), and two use a group of small robots (Minibuilders and Multiple robot printers) [3].

Fig. 11 (a) and (b) show images of gantry and robotic arm 3D printers, respectively.

The two printing systems have limitations; for example, the gantry system can present implementation challenges of transport, installation, and size. The robotic arm system, on the other hand, has limitations regarding the reach of the arm, which is usually limited to 3 m [83].

Other types of printers have also been identified [27,35,44,45,47,48,61,62,75], in delta and polar configuration (Fig. 12 [84]), which, despite the similarity, are not gantry printers. The printers identified in these studies are smaller and produced commercially to be used in other applications but were adapted to serve for studies in civil construction applications. Some printing systems built in the laboratory did not show identification of the type of printing system to which they belonged. These adapted and/or built systems generally have lower costs. Some authors also simulated the 3D printing process [32–34,51,69].

In addition to the challenge of determining the mix design correctly, the use of 3D printing presents another complexity: the presence of several variables in the process and design, which vary from equipment to equipment and can be adjusted, within the limits of the printer, for each type of material. Thus, one must define parameters such as print speed, print interval between layers, nozzle height during printing, path of the printer, flow rate, etc. These parameters will have direct effects on dimensional accuracy, mechanical performance, and bonding between layers of the printed object [9,28,37]. For the printing process to be successful and optimized, mastering the equipment-material interaction is essential [9].

The print speed of the studies varied between 3 mm/s and 90 mm/s. The lowest speeds have been identified in small printers, which are associated with their smaller dimensions and smaller feed and flow systems, which causes the printer to have to work at slower speeds.

The circular nozzles ranged in diameter from 610 μm to 50 mm. Regarding the rectangular nozzles, the nozzle area varied between

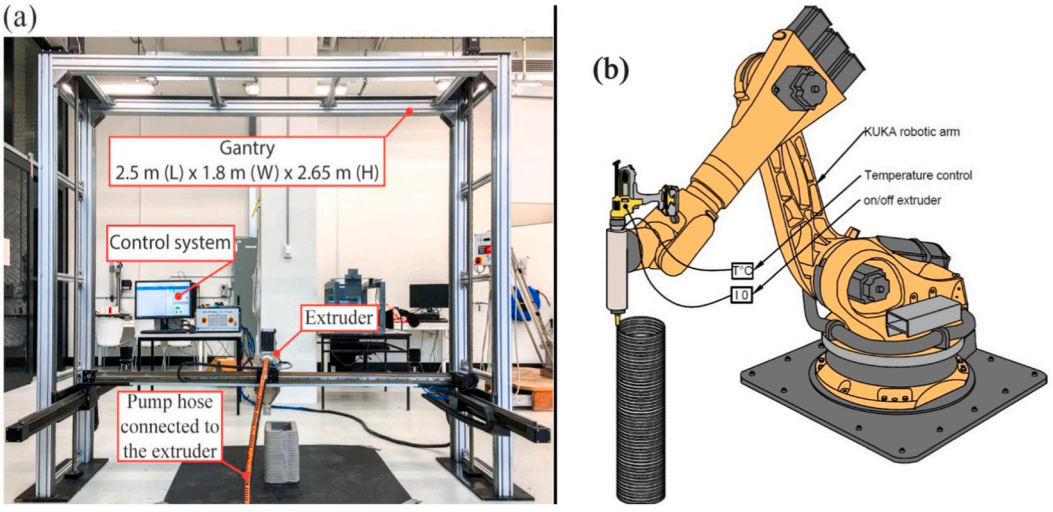

Figs. 11. 3D printers: (a) gantry (adapted from Ref. [38]) and (b) robotic arm (adapted from Ref. [82]).

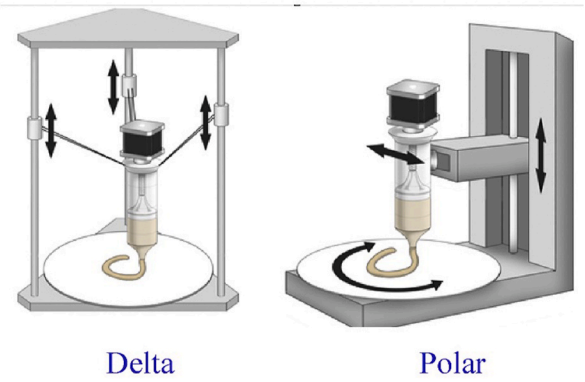

Fig. 12. Illustration of printers with Delta and polar configurations. Adapted from [84].

80 mm^2 and 450 mm^2, with the lowest height of 4 mm and the highest of 20 mm, while the smallest width was 10 mm and the largest 40 mm.

Nozzle dimensions also affect the behavior of the printed object, for example, nozzles with larger diameters generate better buildability for the material, while smaller nozzles can produce objects with better detailing [53].

Ma et al. [64,65] analyzed how to reduce the weight of the structures without causing a decrease in mechanical performance. For this, the authors printed the AAMs in different structural designs, more complex, using a small printer, with a diameter of 800 μm [65] and 600 μm [64]. The use of the smaller dimensions of nozzles identified in the studies came from the need to print complex and detailed structures.

As the market for 3D printers for construction is also recent, commercially purchased printers, adapted printers, and built printers have been identified. This generated a variation in the size and operating mechanism of the printers, which was reflected in the variation in nozzle size and speed. In addition, the mix designs used, and the tests selected to analyze the printed objects also influenced the determination of the parameters, but in a less expressive way.

3.2.1.8. Correlation between different analyses and printing properties. Several studies have indicated the feasibility of successful 3D printing through optimized mix designs with predetermined analyses [23,36,42,46,50,52–54,67]. However, the absence of established standards for evaluating parameters like printability, extrudability, and buildability has led some authors to propose correlations between results from other tests and these parameters. It's crucial to highlight that optimal printing properties can vary based on the specific printing system being utilized.

Alghamdi, Nair, and Neithalath [55] observed that the initial setting time of the mixtures is a property that could be used to estimate the printability window (period of time that the mixture is extrudable), but more studies would be needed to determine the proportion between them. The authors also determined a range of slump (mm) and yield stress (Pa) values, combined, to characterize the mixtures as non-printable and printable, that is, mixtures that are extrudable and buildable, according to the limits of the printer used in the study. The mixtures considered printable presented yield stress between 150 and 700 Pa and slump between 0 and 20 mm.

Tran et al. [42] classified different mix designs of AAMs based on the tests of slump, slump flow, and printing of small filaments; from these tests it was possible to determine a range of slump (15–30 mm) and slump flow (210–240 mm) suitable for 3D printing, which were tested in actual printing tests, showing that it was possible to use simple analyses to determine a printing region.

Ranjbar et al. [35] presented a rheological analysis protocol that can model the hardening evolution of the material during and after its deposition. In this protocol, the authors quantified the yield stress of the material at the origin by a linear fit extrapolation of the green strength; the value of the calculated yield stress was used to predict the printability of the material. If the material has a calculated yield stress lower than the theoretical stress state in the printed structure, it is predicted that it will not be able to sustain its gravitational stress, that is, it is too fluid for printing.

Archez et al. [63] showed that one can use the key characteristics of the material, i.e., yield stress and working time, and associate them with the process parameters (nozzle speed, printing path, and layer height) to predict the time required between printed batches and print a structure without the use of organic additives and achieving both a good layer bond and sufficient resistance to settlement.

3.2.1.9. Properties of printed samples in comparison with casted samples. When comparing 3D printing to traditional casting, there was no consensus on the mechanical performance. In general, printed samples exhibited anisotropic behavior, meaning their mechanical characteristics varied based on the loading direction concerning the printing direction [21,22,27,37,38,40,41,43,48,52]. However, when similar mix designs of AAM and OPC were compared, the anisotropic degree decreased. While OPC-based mix designs ranged between 38% and 105%, AAM presented values between 3% and 20% [51].

The fresh properties of materials have an impact on the mechanical properties. Studies by Albar et al. [53] and Chougan et al. [52] indicated that in 3D printing, this bond between fresh and hardened states becomes more pronounced. This observation stems from the variations seen in the strength differences between traditionally casted and printed samples, as illustrated in Fig. 13 (a) and (b) [52]. In Fig. 13 (a) and (b), each number after the inscriptions PM (printed) and CM (casted) represents a different mix design, involving varied

contents of fly ash (60–70%), GGBS (15–35%), silica fume (5–15%), and aggregate granulometric distribution.

In Fig. 13 (b), one can observe mix designs with a large difference in the mechanical performance of compressive strength between what was casted and printed (M1 and M2), mix designs that presented similar performance (M5 and M6), and mix designs with smaller differences (M3 and M4). The same occurs for flexural strength -Fig. 13 (a), but for different mix designs.

The same phenomenon occurred in the study by Albar et al. [53], in mix designs of AAMs based on fly ash, GGBS, and silica fume, activated by sodium silicate and hydroxide. This variation in the difference in mechanical behavior between printed and casted samples with the same mix design is due to the characteristics in the fresh state of these mix designs, since worse forming conditions generate samples with higher porosities, heterogeneities, and defects, impairing their mechanical performance in a more pronounced way, compared to casted samples.

In both studies by Albar et al. [53] and Chougan et al. [52], the printed samples showed, in general, lower mechanical performance than traditionally casted samples in terms of compressive and flexural strength.

Bong et al. [38] compared 3D printed and traditionally casted samples of an AAM based on fly ash and GGBS. They reported that the printed samples had higher porosity (21.4%) compared to the casted ones (14.5%), mainly due to voids formed during the layer deposition process, situated between the layers. This increased porosity affected the compressive strength of the printed samples, resulting in lower values (10–27% decrease) compared to the casted ones, depending on the direction of the applied load. Additionally, the flexural strength varied with the load direction: the X direction, where the load aligned with the interfaces between layers, had the weakest strength (3.5 MPa) compared to the Y and Z directions (8.4 and 7.9 MPa, respectively). This reduction in the X direction was due to the load application occurring within the plane of interfaces between multiple layers, where most of the pores are concentrated, consequently weakening the flexural strength. The casted sample reached a strength of 6.4 MPa.

Panda et al. [37] also compared the compressive strength of one-part AAM based on fly ash and GGBS in three different directions regarding the printing direction, with casted samples. The printed samples obtained compressive strengths of 28.3, 25.9, and 24.3 MPa, the first being parallel to the printing direction and the last two, horizontal perpendicular and vertical perpendicular, respectively. The casted sample obtained a strength of about 26.5 MPa. All samples had 28 days of curing. In the study by Panda, Unluer, and Tan [25], the samples printed with fly ash, GGBS, and silica fume obtained a compressive strength of 18.4 MPa after 7 days of curing, while the casted samples obtained the average value of 16.2 MPa.

Bong et al. [41] studied strain-hardening one-part AAMs based on GGBS and fly ash, with incorporation the of PVA fiber. Regarding compressive strength, printed composites presented strengths 6–25% lower than casted composites, depending on the type of cure and direction of loading. However, concerning the flexural test, the printed samples presented modulus of rupture (MOR) and deflection at peak load of the MOR (δ_{MOR}), respectively, 16 and 65% higher than the casted samples for composites with ambient cure; concerning those with thermal cure, the increase in MOR and δ_{MOR} was 51 and 57 percent, respectively. The authors related this improvement to the fiber alignment of the samples printed parallel to the print path and perpendicular to cracks, increasing their bridging efficiency, while for casted composites, the fibers were more randomly distributed. Regarding ductility index and average work-to-fracture, the printed samples also showed better flexural performance than the casted samples.

Regarding sample density, in the study conducted by Panda et al. study [21], with AAMs based on fly ash, GGBS, and silica fume activated with potassium silicate and hydroxide, and in the one conducted by Panda et al. [24], focusing on AAMs based on fly ash and GGBS activated with potassium silicate, the printed samples showed higher values of density. The slight density increase in printed samples could result from the material formation via extrusion, allowing mechanical compaction while passing through the nozzle.

Chougan et al. [52] investigated six different AAM mix designs, varying fly ash, GGBS, silica fume content, and sand granulometric distribution. In four mix designs, printed densities were higher than casted ones, while in two designs, casted samples showed higher densities than printed ones. Densities ranged between 2.04 g/cm^3 and 2.27 g/cm^3, with both minimum and maximum densities observed in printed samples. The lower density in the printed samples of the two mix designs was attributed to their fast setting time, hindering composite compaction during extrusion.

3.2.1.10. Influence of printing parameters on the behavior of composites. Printing parameters play a crucial role in shaping the

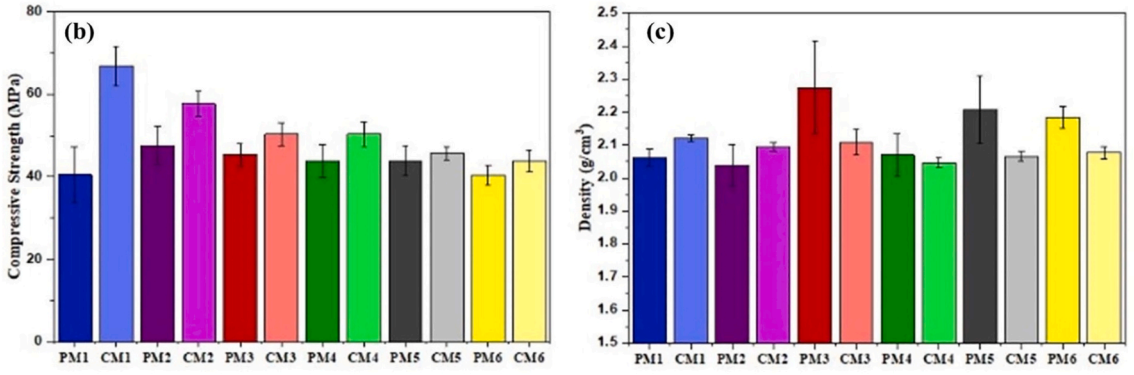

Fig. 13. Mechanical performance of PM (printed) and CM (casted) geopolymers, (a) flexural strength, (b) compressive strength [52].

rheological and mechanical characteristics of printed composites. As reported by Panda et al. [24], the properties of AAM printing and interlayer bonding are significantly influenced by parameters like layer interval, print speed, and nozzle height. In their investigation on AAM layers (fly ash, GGBS, and silica fume), the authors varied the printing interval from 1 to 360 min. Tensile bond tests revealed that longer intervals between layers resulted in weaker interlayer bonds. Moreover, the authors also varied the nozzle speed (printing) in 70, 90, and 110 mm/s, showing similar tensile bond strengths. The 70 mm/s speed slightly outperformed at 1.7 MPa, while the 110 mm/s speed recorded slightly lower at 1.5 MPa. Additionally, altering the nozzle height from the printing surface, known as nozzle standoff distance, impacted the tensile bond strength. Standoff distances of 0, 2, and 4 mm exhibited bond strengths of 2.3, 1.8, and 1.5 MPa, respectively.

Panda et al. [21] also reported a decrease in tensile bond strength with the increase in printing interval between layers from 0 to 20 min.

The increase in the interval between the deposition of the layers can also result in diminished mechanical performance during flexural testing due to weaker bonding between the layers [33].

The print path affects the mechanical properties of composites. Li, Wang, and Ma [49] compared three types of print paths in the production of the samples: the concentric path "A" and the zigzag crosshatch paths "B" and "C" (90 ° rotated to each other). The AAMs tested were one-part based on fly ash, GGBS, and silica fume, without reinforcement (N) and reinforced with a continuous steel micro-cable (F). For the samples without reinforcement, different values of compressive strength values were obtained for each path, with 23.2 (A), 27.6 (B), and 29.2 (C) MPa, while the reinforced samples obtained 25.5 (A), 41.5 (B), and 39.1 (C) MPa. The shear strength averages were higher for the samples printed by path "A" both for the non-reinforced (7.93 MPa for A, 3.57 MPa for B, and 3.89 MPa for C) and the reinforced (10.91 MPa for A, 5.77 MPa for B, and 5.10 MPa for C); the same occurred for the average values of ultimate tensile strength, obtaining values of 2.57 (A), 1.44 (B), and 1.96 (C) MPa for the non-reinforced samples and of 4.69 (a), 3.72 (B), and 1.69 (c) MPa for the reinforced ones. Thus, it's possible to observe that for micro-cable reinforced composites, the variation in results obtained between printing paths was more prominent.

Muthukrishnan, Ramakrishnan, and Sanjayan [39] noted an interdependence between speed and mixing time in the yield strength development rates of AAMs based on fly ash and GGBS, activated with sodium silicate and hydroxide. For example, at a speed of 300 RPM, the average yield strength development rate reached after 60 s was 548 Pa/s; for a speed of 750 RPM, after 15 s, an average yield strength development rate of 598 Pa/s was reached, that is, the increase in speed can be used to reduce the mixing time and reach the same yield strength, and vice versa.

3.2.1.11. Influence of temperature on the behavior of composites. Muthukrishnan; Ramakrishnan; Sanjayan [44] studied the use of microwave heating in the printed composites in the fresh state. The authors evaluated the heating of 5, 10, and 20 s in one-part AAMs based on fly ash and GGBS. For heating times of 10 s, there was an increase in bond strength of 132% (7 days of cure) and 87.5% (28 days), compared to the sample without heating. The Young's modulus showed a substantial increase of 606.8%. However, for 20 s, there was a decrease in bond strength of 43% (7 days) and 29.5% (28 days) compared to the sample without heating. Heating causes a loss of moisture on the surface, and for 10 and 20 s, there is a loss of 28 and 71%, respectively. The sample heated for 20 s also showed high stiffness and loss of malleability, which added to the high moisture loss, caused the lowest bond strength. The optimal heating time was defined as 10 s, since it benefited the reaction process with heat, but did not impair the bond between layers. In this optimal time, the AAMs were able to obtain 100% structural recovery in the rheological test.

Souza et al. [61] studied the preheating of two mixtures of metakaolin-based AAMs activated with sodium hydroxide and silicate. The authors varied the molar oxide ratios of the mixtures. At first, the two presented yield stress outside the buildability zone (below 350 Pa). For the mixture called "A," the stiffening, tested by the Vicat test, occurred mainly between 45 and 90 min; for the mixture called "C," there was no stiffening until 90 min of the test; in the printing test, both mixtures showed excessive flowability. Thus, the authors heated the mix designs after mixing at 50 °C for different times, between 10 and 30 min, and then mixed them again, to break any clusters that may have formed. Samples "A" and "C" became printable after heating times of 12.5 and 27.5 min, respectively.

Muthukrishnan, Ramakrishnan, and Sanjayan [39] studied the influence of released heat on the exothermic reaction of NaOH in the yield strength of AAMs based on fly ash and GGBS activated with sodium silicate and NaOH. For this, two mixing processes were carried out for AAMs with the same composition: in the first, the activator solution (silicate and hydroxide) is added to the dry materials at 25 °C; in the second process, NaOH is mixed to the dry materials and then the solution with sodium silicate is added. After 20 min of mixing, the sample produced by the first process reached only 400 kPa of yield strength, while the sample produced with the second process reached more than 1000 kPa, but presented a drop of 38 and 14% in compressive strength after 1 and 28 days, respectively, which was attributed to the shrinkage of the mixture in the fresh state, due to the exothermic reaction and due to incomplete dissolution of NaOH during mixing, which later becomes empty when NaOH dissolves completely.

Similarly, temperatures lower than room temperature also influence the behavior of composites. In the study by Archez et al. [62] there was no consolidation of the material based on metakaolin and Callovo-Oxfordian argillites (calcined at 650 °C) printed at a temperature of 8 °C, with a relative humidity of 93%.

The curing temperature and duration also caused variations in the mechanical performance of the samples for compression and flexural tests. Alghamdi, Nair, and Neithalath [55] cured different mix designs of AAMs at 23 °C for 28 days and compared their mechanical behavior (flexural and compression) with cure performed at 70 °C for 24 and 48 h. The results are shown in Fig. 14 (a) and (b), where $F_{85}L_{15}$ e $F_{70}L_{30}$ is composed of different proportions of fly ash and limestone, $F_{50}S_{30}L_{20}$ is composed of fly ash, limestone, and GGBS and $F_{50}S_{30}L_{19}A_1$ is similar to $F_{50}S_{30}L_{20}$ but with the incorporation of 1% alumina powder.

Bong et al. [41] compared strain-hardening one-part AAMs based on GGBS and fly ash, with PVA fiber incorporation, cured for 28

days at room temperature with composites cured for 24 h at 60 °C, followed by room temperature curing, completing seven days of curing. When subjected to the compressive strength test, the printed composites cured only at room temperature showed 12–25% higher values, depending on the direction of loading. Regarding the flexural test, the reverse occurred: the samples printed with thermal cure presented LOP, δ_{LOP}, MOR, and δ_{MOR} 23, 17, 36, and 6% higher, respectively than thermally cured samples. The better mechanical behavior was linked to slower geopolymerization of composites with room temperature curing, generating a denser microstructure, while the worse flexural behavior was attributed to the presence of tensile eigenstresses in these composites.

Thus, based on the studies of Alghamdi, Nair, and Neithalath [55] and Bong et al. [41], it's possible to conclude that curing time and temperature affect AAMs differently, depending on the constituent materials and their variables. For instance, heat treatment induced extensive microcracking in the $F_{50}S_{30}L_{20}$ and $F_{50}S_{30}L_{19}A_1$ mixtures due to the high shrinkage of slag-containing alkali-activated binders. Additionally, depending on the reaction mechanisms and time of reaction, the curing type can also lead to differences in the same mix design across various tests. A specific curing method may promote greater gel formation. However, it can also induce internal stresses and based on the applied load, might positively or negatively affect the material's mechanical behavior.

3.2.2. *Powder-based systems*

As in extrusion printing, in powder-based systems, one must also control different parameters such as the properties of the powder, activator, and printing parameters [85]. The deposited layers must also have sufficient green strength to withstand subsequent layers without significant deformation or collapse [6]. One of the limitations of powder-based systems is the compatibility between the material and the printer, regarding flowability, particle size, and wettability [5]. The saturation of the binder is of great importance in the powder-based system, affecting the activator/powder interaction and resembling the water/binder ratio for cementitious matrices. If the saturation is too high, there will be binder leakage, and if it is too low, it can generate a very low green strength due to low binding between the particles [85]. Obtaining the desired dimensional accuracy for the application of powder-based systems in complex structures can also be challenging [86].

3.2.2.1. Materials. Table 12 displays the materials employed as precursors, activators, inert components, and additives, along with the respective studies in which they were utilized.

Precursors were classified based on combinations of constituent materials—silica and/or alumina sources. Some materials alone may not act as precursors, but when combined, they contribute to the formation of the main reaction products. Since most authors only used the term "slag" and did not provide further details, it was also decided not to specify it as GGBS in Table 12. As this is a different matrix than those of extrusion-based systems, the term "inert component" was chosen rather than aggregate/filler.

For this category of printing process, the most used precursor in the studies was slag. The material was the main precursor in 57% of the studies. Regarding activators, sodium silicate remains the most used activator, which was also associated with other activators such as sodium hydroxide.

The only inert component used was sand, which was incorporated in 6 of the 7 studies. Sand granulometries of up to 0.17 mm were identified, but some studies did not specify the value. The binder/sand ratio ranged from 0.05 to 4, but some values were also not specified in the studies; it is important to note that these values were identified considering the entire study, from preliminary tests to the final stages.

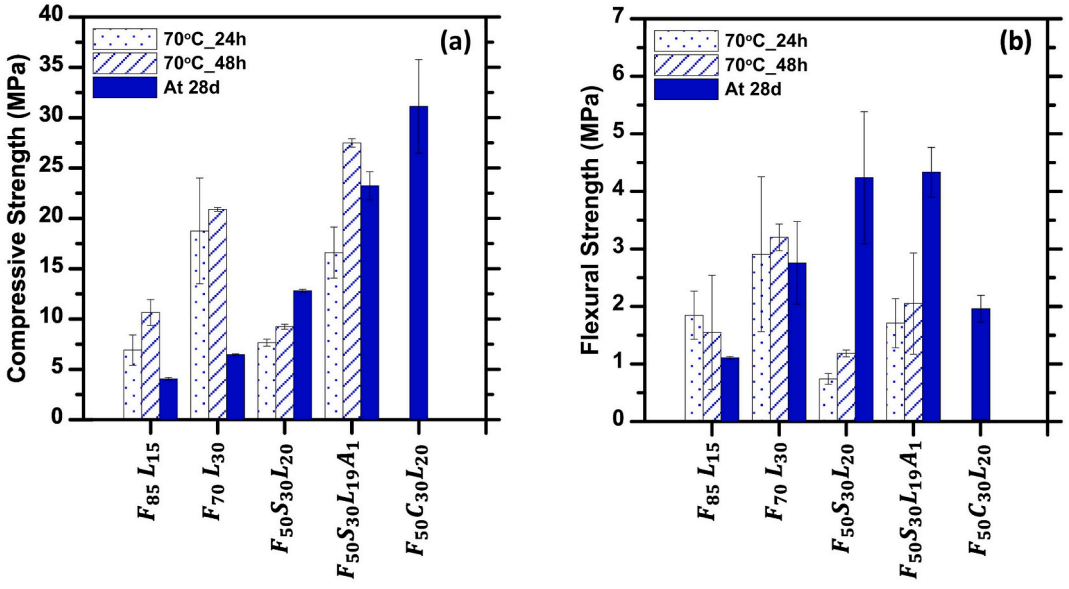

Fig. 14. (a) Compressive strengths, and (b) flexural strengths of different mix designs after subjecting to different curing regimes [55].

Table 12
Materials used in the analyzed studies and their respective works – Powder-based systems.

Precursors	Metakaolin	[5,87]
	Slag	[6,85,86]
	Fly ash	[86,88]
	Fly ash + slag	[7,86]
	Fly ash + slag + $Ca(OH)_2$	[7]
Activators	Sodium Silicate	[5–7,85,86,88]
	Sodium hydroxide (NaOH)	[5,6,86–88]
	Silica gel	[87]
Inert component	Sand	[5–7,85–87]
Additives	Solvent	[6,7,85,86]

About 57% of the studies used solvent in the printing process, but Park et al. [7] showed that the use of pure water as a reactive agent binder generates a 10% improvement in mechanical behavior.

3.2.2.2. Influence of materials on the 3D printed AAM. Regarding the influence of the constituent materials of AAMs, studies have identified the impact of variations between fly ash/GGBS ratios [86], metakaolin/sand ratios [5,87], and the influence of calcium hydroxide addition [7].

It was observed in the study of AAMs based on GGBS and fly ash [86] that the increase in fly ash influenced the time required for binder penetration, diameter of spread of the binder droplet, depth of penetration of the binder droplets, which meant that the properties of the powder, such as density, size, and shape of the particles influence the penetration behavior of the binder. The content of fly ash also affected the linear dimensional accuracy and compressive strength.

The increase in the fly ash content caused an increase in the time required for binder penetration, from 335 ms (100% GGBS) to 580 ms (100% fly ash). In addition to presenting the shortest penetration time, the AAMs with only GGBS and without fly ash presented a greater diameter of spread of the binder droplet (1.95 mm), compared to AAMs with incorporation of contents of 25% (1.82 mm), 50% (1.72 mm), and 75% (1.67 mm) of fly ash. However, they presented the lowest depth of penetration of the binder droplets, with a value of 2.10 mm, while the AAMs with 25, 50, and 75% fly ash obtained values of 2.46, 2.78, and 2.90 mm. It was not possible to measure the values of droplet spreading diameter and droplet penetration depth for AAMs based on 100% fly ash due to the weak strength of granules, not supporting the pressure of the de-powdering process [86].

The increase in the fly ash percentage decreased the linear dimensional accuracy of the green sample (without post-processing procedures) in the Z direction, the mean error value was 0.23 for the sample based on 100% GGBS and 0.38 mm for the sample with 75% fly ash, which may be connected with the differences in powder bed structure and level of powder/binder reactivity; for the X and Y directions, there was no great influence of fly ash. For samples with post-processing procedures, the influence of fly ash varied depending on the curing solution applied. Regardless of the direction of the loading or whether or not the sample has undergone post-processing procedures, the increase in fly ash content always leads to a decrease in the compressive strength of the samples, but the quantification of this decrease varies according to the post-processing procedure and loading direction. The samples with 25% slag and 75% fly ash, submitted to the post-processing procedure, were dissolved in the curing solutions and were not tested [86].

Voney et al. [87] compared different metakaolin/sand ratios (0/100, 10/90, 20/80, 40/60, 60/40, 80/20, and 100/0) in AAMs activated with a solution of NaOH and silica gel. The authors compared the dry drops produced by the deposition of 10 μl of alkaline solution in loosely packed powder beds and observed that for values greater than 20% of metakaolin, the higher its content, the smaller the volume of the resulting drops, which was attributed to the lower packing of the material with the increase in metakaolin, which shows higher voids, thus the same amount of liquid finds place in a smaller powder volume. It was also determined that the minimum of metakaolin required for the formation of strong AAMs was 20% since smaller amounts fell apart when submerged in water; in addition, X-ray microtomography images showed that for values lower than 20% of metakaolin there is no complete densification of the internal structure of the droplet.

Rehman and Sglavo [5] also compared different sand/metakaolin ratios (from 1:1 to 8:1, by mass) and rated the materials for flowability by visual inspection upon the deposition of 40 layers. For metakaolin/sand ratios between 1:1 and 1:5, the materials were classified as not flowable; for the ratios 1:6 and 1:7, they were partially flowable that is, able to flow, but presented inconsistencies in the layers; the only ratio considered flowable was 1:8. That is, the increase in the content of metakaolin to sand decreases the flowability of the mixture since metakaolin is a very cohesive material.

Park et al. [7] studied different additions of calcium hydroxide (between 7.5 and 13.12% in relation to the mass of the precursors) in AAMs composed of 80% GGBS and 20% fly ash. It was observed that the bulk density decreased slightly with increasing $Ca(OH)_2$ content; the sample without the material showed a density of 1.74 g/cm^3, while the sample with the highest $Ca(OH)_2$ content (13.12%) obtained 1.69 g/cm^3. The water absorption decreased, and the compressive strength of the composites increased with the increase of calcium hydroxide incorporation. The AAMs without hydroxide obtained 1.90% absorption and 13.56 MPa, while the AAMs with 13.12% incorporation obtained 1.56% and 24.34 MPa. However, the increase in $Ca(OH)_2$ generates an increase in discharged powder, which can lead to damage to the operation of the 3D equipment.

3.2.2.3. Methodology. Table 13 shows the analyses adopted, dividing them into 3D pre-printing analyses, curing type, and 3D post-printing analyses.

Although less explored in publications, the powder-based category exhibits variations in the analyses employed by authors, with the vast majority (86%) conducting solely compressive strength tests.

Voney et al. [87] studied the behavior of droplets by simulating the 3D process, in which a pre-established volume of the solution was poured into the powdery mixtures. From this experiment, the authors determined the ratio of liquid to solid, the theoretical molar ratios of Si/Al and Na/Al, the height and final diameter of the drop, the average volume of the dry drop, the mass of the dry drop, powder packing in the drop, and qualitative study of the microstructure using X-ray microtomography.

Xia, Nematollahi, and Sanjayan [86] analyzed droplet behavior by studying droplet penetration, determining penetration time, penetration depth, and spreading diameter. They used a custom-made apparatus and determined the time taken for the droplet to fully penetrate the powder bed through analysis with a high-speed video camera. The depositability of powders was analyzed using digital image processing techniques. About 70% of the authors performed post-processing of the printed samples in their studies. Xia, Nematollahi, and Sanjayan [86] performed the post-processing of the samples at 60 °C for seven days studying three different alkaline solutions, in which the combinations of saturated anhydrous sodium metasilicate, sodium N silicate, and sodium hydroxide (NaOH) were varied.

Nematollahi, Xia, and Sanjayan [6] used solutions based on sodium silicate and potassium in the post-processing; two types of sodium silicate and two types of potassium silicate were analyzed. The post-processing was divided into two distinct groups: with heating and room temperature. The samples with heated cure were immersed in alkaline curing environment at 60 °C for seven days, after which they were stored at room temperature until the day of the test. The samples with room temperature cure were immersed in alkaline medium at 23 °C for seven and 28 days, after which they were stored at room temperature until the day of the test.

Xia, Nematollahi, and Sanjayan [85] immersed the green samples in saturated anhydrous sodium metasilicate solution and placed in an oven at 60 °C for 7 days.

Xia and Sanjayan [88] varied the temperature (25, 40, 60, and 80 °C) for the same curing environment to determine the optimal temperature (60 °C). Then the optimum temperature was used to study the variation of the curing environment in compressive strength. Seven types of curing environments were analyzed: one tap water, three alkaline solutions, and three fly ash-based geopolymer slurries.

Park et al. [7] explored various ratios of Na_2SiO_3/NaOH and different moles of NaOH in their study. The researches prepared a total of 21 post-processing storage solutions by altering Na_2SiO_3/NaOH ratios (1, 2, 3, 4, and 5) and moles of NaOH (1, 2, 3, 4, and 5) using liquid sodium silicate (comprising SiO_2 28.2%, Na_2O 9.3%, and H2O 65.5%) along with 98% NaOH. Additionally, in contrast to other studies, a vacuum impregnation of the composites was performed in the post-processing.

3.2.2.4. Influence of printing parameters on the 3D printed AAM. Regarding printing parameters, Voney et al. [87] explored the correlation between power bed saturation, dimensional accuracy, and compressive strength in metakaolin-based AAMs activated with NaOH and silica gel. The authors observed that higher saturation levels led to increased compressive strengths. At a 46% saturation, the strength was approximately 1 MPa, while at 108%, it reached about 8 MPa. Concerning dimensional accuracy, saturations exceeding 70% resulted in a dominance of the liquid phase, consequently reducing dimensional accuracy.

Xia, Nematollahi, and Sanjayan [85] also observed a lower dimensional accuracy with increasing binder saturation level; in addition, the samples showed anisotropic behavior and the lowest linear dimensional accuracy was always observed for the dimensions in the Z direction (thickness). For the sample with binder saturation level of 75%, there was a linear dimensional error of

Table 13
Methodologies used in the analyzed studies - Powder-based systems.

.	Flowability of the powder mixtures	[5]
3D pre-printing analyses	Power bed packing	[87]
.	Droplet behavior	[86,87]
	Determination of powder bed porosity	[86]
	Determination of the particle size distribution of the powdery geopolymer	[86]
	Determination of powder bed density in process	[86]
	Determination of the true/bulk density of the powder bed	[86]
	Powder depositability analysis	[86]
Curing type and post-processing	Immersion in a curing environment with temperatures equal to or above 40 °C	[6,85,86,88]
	Ambient temperature, no post-processing	[5,86,87]
	Vacuum impregnation with immersion in the curing environment, followed by immersion in the curing environment at 70 °C	[7]
	Immersion in a curing environment at ambient temperature	[86,88]
.	Flexural test	[5]
3D post-printing analyses	Dimensional accuracy	[5,85,86]
.	XRD	[5]
	Determination of apparent porosity of printed composites	[6]
	Compressive strength test	[6,7,85–88]
	Nuclear magnetic resonance (NMR)	[87]
	Determination of water absorption of printed composites	[7]
	Determination of bulk density of printed composites	[7]
	Analysis of the permeation depth of the post-processing solution	[7]
	Scanning electron microscopy with energy dispersive X-ray spectroscopy	[87]

0.04, 0.04, and 0.15 mm for the X, Y, and Z directions, respectively, while for the samples with binder saturation level of 170%, for the same directions, the errors were 0.21, 0.40, and 0.66 mm. The anisotropic behavior was accentuated with the increase of the binder saturation level in relation to dimensional accuracy and compressive strength. The mechanical behavior improved as the binder saturation level of the samples increased with or without post-processing. For the green samples, the sample with 75% saturation reached 0.4 MPa (X direction) and 0.3 MPa (Z direction), while the sample with 170% saturation reached 1.3 MPa (X direction) and 0.8 MPa (Z direction). For the samples with post-processing submerged in saturated anhydrous sodium metasilicate solution with the same saturation levels, the values obtained in the X direction were 12.9 MPa (75%) and 19.3 MPa (170%), and in the Z direction, 11.8 MPa (75%) and 17.2 MPa (170%).

Thus, there is a contrast between the mechanical properties and dimensional accuracy concerning the saturation level. As saturation increases, mechanical strength rises, yet dimensional accuracy decreases.

Rehman and Sglavo [5] varied the binder flow rate between 103 and 181 mg/s for AAMs based on metakaolin, activated with sodium silicate and hydroxide. Regarding dimensional accuracy, there was no difference in the values of printed length and width; all samples obtained the values of computational design, but the increase in flow rate also generated an increase in thickness; the sample with binder flow rate of 103 obtained the same computational value (40 mm), while the sample with higher flow rate (181 mg/s) obtained 44 mm. The authors pointed out that, for these study conditions, gravity-drive downward permeation was much more important than capillary diffusion. Regarding the flexural strength, it was not possible to draw an exact relationship between the increase and decrease of the binder flow rate and mechanical strength; for this study, the maximum and minimum values were obtained with binder flow rates of 135 (4.4 MPa) and 107 mg/s (2.3 MPa), respectively.

In the study by Voney et al. [87], printed and casted samples were compared. The defects generated during printing, the heterogeneity of the samples, and the higher porosity caused the printed samples to obtain lower compressive strengths (5.3 MPa) than the casted samples (35 MPa), even with similar densities (1.6 g/cm^3 for the printed and 1.8 g/cm^3 for the casted). While in the casted samples, the liquid/solid ratio depends only on what was added to the mixture, in the 3D printing process this ratio also depends on the penetration behavior and the distribution of the liquid in the powder bed. The refinement of the print parameters and composition of the AAMs might help the improvement of the performance of printed samples. The authors propose a mix design method in which, based on the composition and packing factor of the bed powder, the composition of the liquid is adapted to obtain the desired Si/Al and Na/Al parameters.

3.2.2.5. Influence of the curing method on the 3D printed AAM. Regarding the influence of temperature on curing, Xia and Sanjayan [88] observed that for fly ash-based AAMs, as the temperature increases (25 °C up to 60 °C), there is an increase in compressive strength. For green samples cured at 25 °C, the samples showed compressive strengths of 2.3 and 3.8 MPa after 3 and 7 days, respectively; the samples cured at 60 °C reached 12.9 MPa (3 days) and 16.3 MPa (7 days). However, for a curing temperature above this value (80 °C), there is a decrease in compressive strength, with 8.5 MPa (3 days) and 10.2 MPa (7 days), results slightly lower than those achieved at 40 °C (9.3 MPa with 3 days and 12.9 MPa with 7 days).

Different studies have indicated significantly improvement in the mechanical behavior for samples submitted to post-processing, with cure immersed in alkaline solutions or alkaline activated slurries [6,7,85,86].

In the study by Xia, Nematollahi, and Sanjayan [85], slag-based AAMs immersed in saturated anhydrous sodium metasilicate solution showed significantly higher compressive strengths than green samples, regardless of loading direction and binder saturation level. For example, for the binder saturation of 100%, the immersed sample reached 16.3 MPa (Z direction) and 15.2 MPa (Z direction), while the green sample reached only 0.9 MPa (X direction) and 0.5 MPa (Z direction).

Xia, Nematollahi, and Sanjayan [86] also compared green samples with three different curing environments for AAMs based on slag and fly ash. The samples were immersed for 7 days at 60 °C in three curing environments: 1) composed of saturated anhydrous sodium metasilicate solution; 2) composed of saturated anhydrous sodium metasilicate solution and 8 M NaOH solution; and 3) composed of sodium silicate solution and 8 M NaOH solution. The highest compressive strength values obtained by the green samples in the X and Z directions were 0.91 and 0.76 MPa, respectively, with 100% slag-based AAMs, while the lowest value obtained by the samples with post-processing was 7.1 MPa (X direction) and 6.1 MPa (Z direction), for AAMs composed of 50% slag and 50% fly ash, immersed in solution 1. The notable discrepancy between the higher strength exhibited by the green samples and the lower strength observed in the post-treated samples highlights the considerable enhancement achieved through post-processing in terms of mechanical behavior.

Nematollahi, Xia, and Sanjayan [6] compared curing environments based on sodium and potassium; there were 4 curing environments studied in total: 2 composed of sodium silicate and hydroxide and 2 of potassium hydroxide and silicate, with different SiO_2/M_2O ratios (M = Na or K). Regardless of the type of cure (thermal or room temperature), slag-based AAMs showed higher compressive strengths when submerged in sodium-based environments.

Park et al. [7] incorporated the step of vacuum impregnation in the post-processing of the samples. Thus, after de-powdering, the printed samples were kept immersed in the post-processing storage solution in a vacuum impregnator until no air bubbles were produced in the printed sample, which took about 10 min. Fig. 15 [7] schematically illustrates how this process works.

The use of vacuum impregnation was effective and increased the permeation area of the solution: for the AAM samples based on GGBS and fly ash, measuring 20 mm^3, the permeation area of the solution without vacuum impregnation was 18.3%. However, for the impregnated samples, the permeation areas reached 100% for pump operating pressures of 0.06 and 0.10 MPa. This was reflected in the compressive strength: the 20 cm^3 samples without post-treatment achieved 0.66 MPa, while those without the impregnation process reached 1.30 MPa. On the other hand, the samples subjected to impregnation at pressures of 0.06 MPa and 0.10 MPa achieved 19.01 MPa and 19.64 MPa, respectively [7].

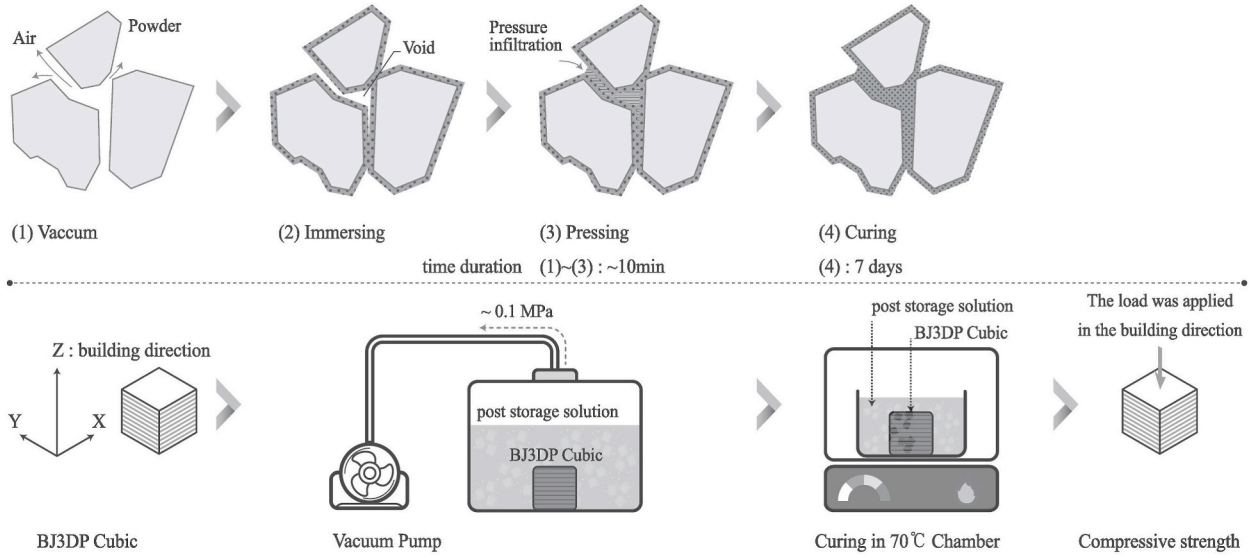

Fig. 15. Visualization of the post-processing via vacuum impregnation [7].

From the data presented in this topic, it was possible to observe that as well as the samples printed by the extrusion-based system, the samples printed by the powder-based system also showed anisotropic behavior in the mechanical results, regardless of the type of curing and post-processing.

4. Discussion

When analyzing the articles, it is possible to identify some challenges to the implementation of 3D-printed AAMs as a commercial construction method. These challenges can be divided into scientific and large-scale. The scientific challenges refer to research topics that can be explored further and to inherent challenges in the AAMs themselves, such as the wide variety of materials that can be used as components. This makes generalizing the properties of this material difficult, requiring case-by-case studies to draw relevant conclusions about the materials.

For instance, a very commonly made generalization is that AAMs are more sustainable materials with lower impacts than OPC-based ones. However, due to the variability of AAM components, this is a statement that should be further investigated.

Liu et al. [89] conducted a life cycle analysis (LCA) to compare the environmental impact of printed and casted AAMs and OPC-based materials. For casted designs, AAMs showed superior environmental performance compared to OPC designs. However, in the case of printed samples, the opposite was observed. The printed OPC mix design displayed better environmental performance than the casted OPC design, while the scenario was reversed for AAMs. In summary, casted AAMs demonstrated better environmental performance compared to casted OPC and also when compared to 3D printed AAMs. The increased environmental impact of printed AAMs is attributed to the higher activator content required to achieve desired printing parameters. Notably, the use of sodium silicate was identified as the primary contributor to the environmental impact of AAMs.

The use of sodium silicate is a major obstacle to achieving sustainability and low environmental impact of AAMs, since it is the most responsible for the environmental burden compared to the other components, despite presenting a small part of the volume [90]. This large emission is linked to its complex and intense production system that involves high temperatures (above 1100 °C) and high energy demand [91,92]. In topics 3.2.1.1. and 3.2.2.1, it was observed that sodium silicate is the most used activator in AAMs for 3D printing for both extrusion and powder-based systems. Thus, the search for alternative activators should be an issue addressed in future studies to achieve the best environmental performance of the desired AAMs. These alternative activators can be derived from industrial or agro-industrial processes and could be combined with traditional activators with lower environmental burden, or activators derived entirely from wastes [93].

Extrusion-based systems 3D printing aims to bring technology, speed, and safety to construction, so printed composites will be subject to weather and climatic variations during printing. As discussed in item 3.2.1.2.4, temperature has a high influence on the reaction process of AAMs, and its influence can vary depending on the constituent materials of the AAMs. Therefore, it is interesting to have more studies on climate variations for AAMs printed on-site. Furthermore, the shrinkage behavior of AAMs is a crucial point of study, particularly in the context of 3D printing, and only one published article has been identified to have investigated this property for extrusion-based systems.

The durability of these materials is also an extremely important research topic, especially in the context of 3D printing, an area that has not received enough attention in studies. While research on AAMs has significantly advanced since its initial publications, there are still many scientific topics to be explored and deepened in these materials, especially considering on-site construction.

Another scientific obstacle to the practical application of AAMs is the variation of tests to evaluate the properties of matrices for 3D

printing. The technical and scientific community is already mobilizing to create a standardization of constructive additive manufacturing. For example, committees created by ISO (ISO/TC 261) and ASTM (F42), which worked in partnership to create the standard "ISO/ASTM DIS 52939 - Additive Manufacturing for Construction — Qualification principles — Structural and infrastructure elements," which was at the draft stage and open to the public for suggestions until mid-December 2022 [94].

The large-scale issues refer to the challenges of actually making these materials applicable as an alternative to traditional construction methods on a global scale. Besides the challenges of the construction method itself, which have been extensively detailed in other reviews solely focused on this subject, AAMs have inherent material-related issues to overcome.

For example, one issue concerning the widespread application of AAMs lies in the commonly used precursor materials. As observed, fly ash has been the most widely utilized precursor, with its prevalence linked to countries with a high number of published works, especially Australia and China, where this material is readily available. However, in regions such as the European Union, there is a trend towards reducing coal usage as an energy source. In South America, except for Colombia, coal consumption for energy production is not substantial [95]. Other materials used as precursors or as components of precursors, such as metakaolin and silica fume, are also extensively utilized in conventional construction, which can create competition. Therefore, it would be advantageous to expand studies into alternative precursors for 3D printing applications.

AAMs' singularity can also pose a challenge, as depending on the activators and precursors used, in-depth studies on the properties of these materials are necessary. For instance, understanding the influence of activator concentrations concerning precursors, identifying which additives are compatible with the system, and if multiple precursors or activators are used, studying the best proportions for the intended outcome is crucial. Certainly, studies on dosage regarding OPC-based materials also take place, but AAMs entail more variables, often showing non-linear results. In this matter, as observed in the articles analyzed in this study, changing the quantity of a specific material can initially increase strength up to a certain concentration. However, beyond that point, reaction mechanisms may change, resulting in diminishing returns. Additionally, the impact of a single activator or additive can vary significantly depending on the predominant precursor used. In summary, AAMs exhibit greater complexity than OPC-based materials. Thus, reviews dedicated to the theme of AAMs applied in additive manufacturing for construction, such as [96–100] are of great importance for gaining a deeper understanding of these variations and identifying key points regarding materials and analytical methods.

5. Conclusion

In this study, a review of 55 articles published between 2017 and 2023 was conducted, with 48 articles related to extrusion-based systems and 7 related to powder-based systems. The main aim of this study is to identify trends related to materials and methodologies in articles focused on 3D-printed AAM. Furthermore, it seeks to highlight the results of these research efforts, providing researchers with insights into potential research opportunities.

In this context, the bibliographic analysis revealed that authors tend to favor terms derived from "geopolymers" over "alkali-activated materials" when referring to the material, despite the prevalence of hybrid system applications in most studies. Research on alkali-activated materials in 3D printing is primarily concentrated in Australia, China, and Singapore, where a robust collaborative network exists among researchers.

Concerning the materials used in mix designs for extrusion-based systems, despite the variability of results depending on the materials used and their respective proportions, the following trends were identified.

- Fly ash is the most used precursor. Its partial substitution by other materials (e.g., GGBS, OPC, silica fume) modifies the properties of AAM and can assist in determining the ideal AAM for the printing protocol used. The use of GGBS affects setting time by accelerating the geopolymerization process, which, in turn, influences the rheological properties of the material. While it enhances mechanical performance, it reduces flowability due to its angular particles. Silica fume does not significantly affect setting time but increases yield stress and enhances thixotropy.
- Different types of activators yield different results depending on the precursor type. For instance, the activation of GGBS with a potassium-based activator shortens the initial setting time compared to sodium-based activation. In contrast, the kinetics of geopolymerization for fly ash with a potassium-based activator proceed more slowly than with a sodium-based activator. In hybrid systems, the use of sodium-based or potassium-based activators can influence geopolymerization time and mechanical strength depending on the precursors and their proportions.
- Additives like CMS, sucrose powder, and similar materials have the potential to extend the open time of AAMs but may worsen their mechanical behavior. Attapulgite clay and its derivatives improve the thixotropy of AAMs.
- Randomly distributed fibers enhance the shape retention of 3D-printed composites but also increases the stiffness of the AAM, which weakens the bond between layers and accentuates composite anisotropy.

In terms of the influence of the printing and post-printing processes on the resulting 3D material, the following trends were observed.

- 3D-printed AAM exhibits anisotropic behavior, but when compared with OPC-based mixtures, the degree of anisotropy was lower, ranging between 3% and 20%, while that of OPC ranged between 38% and 105%.
- The characteristics of the printed material in the fresh state significantly influence the mechanical behavior of the cured material. Worse forming conditions generate samples with higher porosities, heterogeneities, and defects.

- Increasing the layer-to-layer printing time and standoff distance weakens the bond between layers and adversely affects the mechanical behavior of 3D-printed AAMs.
- The effect of curing type and time vary depending on the materials present in AAMs. For instance, samples composed of fly ash and limestone achieved the highest compressive and flexural strength values with thermal curing after 48 h, while samples containing fly ash, limestone, and GGBS showed better results with cure at 23 °C.

For powder-based systems, the following trends were observed.

- In contrast to extrusion-based systems, slag was the most frequently used precursor in powder-based system articles, but sodium silicate remained the most common activator.
- Partial replacement of slag with fly ash increased binder penetration time and depth and reduced the spread diameter of the binder droplet and compressive strength.
- Regarding printing parameters, an increase in power bed saturation led to higher compressive strengths but reduced dimensional accuracy, resulting in a more pronounced anisotropic behavior of printed samples.
- Post-processing of samples improved mechanical behavior, whether through immersion in alkaline solutions or alkaline-activated slurries.

Thus, based on the analysis of the articles, the authors believe that the following research topics would be of great interest to the development of this research field.

- Durability of AAMs applied to 3D printing.
- Search for alternative activators to replace sodium silicate.
- Search for alternative precursors.
- Studies on the shrinkage of 3D-printed AAMs
- Influence of climatic variations on AAMs for on-site 3D construction

Compared to the use of Portland cement-based materials in 3D printing, AAMs present greater complexity as they constitute an extremely diverse group of materials, leading to significant variability in their characteristics in both fresh and hardened states. For instance, the standardized determination of setting time using the Vicat apparatus revealed a range of initial setting times spanning from approximately 7 min to over 480 min. The exact value was not determined, with a recorded initial setting time of 360 min.

Moreover, the rheological, physical, and mechanical characteristics required for materials in the construction industry via additive manufacturing also display significant diversity. Depending on factors such as the type of equipment used, the nature of the construction project, and considerations related to economics, environment, and desired performance. AAMs, as an alternative, offer a wide range of options that can be tailored to optimize desired properties, potentially reducing costs and environmental impacts. The combination of AAMs with 3D printing introduces the prospect of revolutionizing traditional civil construction by integrating technology and sustainability.

Data availability

Data will be made available on request.

CRediT authorship contribution statement

Maria Júlia Bassan de Moraes: Writing – original draft, Writing – review & editing, Supervision, Resources, Methodology, Formal analysis. **Ester Yukimi Nagata:** Writing – original draft, Writing – review & editing, Methodology, Conceptualization. **Afonso José Felício Peres Duran:** Writing – review & editing, Formal analysis. **João Adriano Rossignolo:** Supervision, Resources, Formal analysis.

Declaration of competing interest

The authors declare that they have no known competing financial interests or personal relationships that could have appeared to influence the work reported in this paper.

Acknowledgements

This study was supported by the São Paulo Research Foundation (FAPESP) [grant numbers #2019/11949–8, #2022/02492–7].

References

[1] M. Ghobakhloo, M. Fathi, M. Iranmanesh, P. Maroufkhani, M.E. Morales, Industry 4.0 ten years on: a bibliometric and systematic review of concepts, sustainability value drivers, and success determinants, J. Clean. Prod. 302 (2021) 127052, https://doi.org/10.1016/j.jclepro.2021.127052.

[2] ISO/ASTM 52900–21, Additive Manufacturing–General Principles– Fundamentals and Vocabulary, 2021, pp. 1–9.
[3] S. Pessoa, A.S. Guimarães, S.S. Lucas, N. Simões, 3D printing in the construction industry - a systematic review of the thermal performance in buildings, Renew. Sustain. Energy Rev. 141 (2021), https://doi.org/10.1016/j.rser.2021.110794.
[4] G.W. Ma, L. Wang, Y. Ju, State-of-the-art of 3D printing technology of cementitious material—an emerging technique for construction, Sci. China Technol. Sci. 61 (2018) 475–495, https://doi.org/10.1007/s11431-016-9077-7.
[5] A. Ur Rehman, V.M. Sglavo, 3D printing of geopolymer-based concrete for building applications, Rapid Prototyp. J. 26 (2020) 1783–1788, https://doi.org/10.1108/RPJ-09-2019-0244.
[6] B. Nematollahi, M. Xia, J. Sanjayan, Post-processing methods to improve strength of particle-bed 3d printed geopolymer for digital construction applications, Front. Mater. 6 (2019), https://doi.org/10.3389/fmats.2019.00160.
[7] K. min Park, K. sung Min, B. chun Lee, Y. sook Roh, Proposal for enhancing the compressive strength of alkali-activated materials-based binder jetting 3D printed outputs, Construct. Build. Mater. 303 (2021) 124377, https://doi.org/10.1016/j.conbuildmat.2021.124377.
[8] A. Siddika, M.A. Al Mamun, W. Ferdous, A.K. Saha, R. Alyousef, 3D-printed concrete: applications, performance, and challenges, J. Sustain. Cem. Mater. 9 (2020) 127–164, https://doi.org/10.1080/21650373.2019.1705199.
[9] V. Mechtcherine, F.P. Bos, A. Perrot, W.R.L. da Silva, V.N. Nerella, S. Fataei, R.J.M. Wolfs, M. Sonebi, N. Roussel, Extrusion-based additive manufacturing with cement-based materials – production steps, processes, and their underlying physics: a review, Cement Concr. Res. 132 (2020) 106037, https://doi.org/10.1016/j.cemconres.2020.106037.
[10] G. Ma, Z. Li, L. Wang, G. Bai, Micro-cable reinforced geopolymer composite for extrusion-based 3D printing, Mater. Lett. 235 (2019) 144–147, https://doi.org/10.1016/j.matlet.2018.09.159.
[11] S.J. Schuldt, J.A. Jagoda, A.J. Hoisington, J.D. Delorit, A systematic review and analysis of the viability of 3D-printed construction in remote environments, Autom. ConStruct. 125 (2021), https://doi.org/10.1016/j.autcon.2021.103642.
[12] International Energy Agency – IAE, Cement Sustainability Initiative – CSI, Technology Roadmap: Low-Carbon Transition in the Cement Industry, 2018.
[13] I. Garcia-Lodeiro, A. Palomo, FERNÁNDEZ-JIMÉNEZ, an overview of the chemistry of alkali-activated cement-based binders, in: F. PACHECO-TORGAL, J. A. LABRINCHA, C. LEONELLI, A. PALOMO, P. CHINDAPRASIR (Eds.), Handb. Alkaliactivated Cem. Mortars Concr., first ed., Woodhead Publishing Limited, United Kingdom, 2015, pp. 19–47, https://doi.org/10.1533/9781782422884.1.19.
[14] C. Ouellet-Plamondon, G. Habert, Life cycle assessment (LCA) of alkali-activated cements and concretes, in: P.C.F. Pacheco-Torgal, J.A. Labrincha, C. Leonelli, A. Palomo (Eds.), Handb. Alkali-Activated Cem. Mortars Concr., Woodhead Publishing Limited, 2015, pp. 663–686, https://doi.org/10.1533/9781782422884.5.663.
[15] L. Lima, E. Trindade, L. Alencar, M. Alencar, L. Silva, Sustainability in the construction industry: a systematic review of the literature, J. Clean. Prod. 289 (2021) 125730, https://doi.org/10.1016/j.jclepro.2020.125730.
[16] J.A. Rossignolo, A.J. Felicio Peres Duran, C. Bueno, J.E. Martinelli Filho, H. Savastano Junior, F.G. Tonin, Algae application in civil construction: a review with focus on the potential uses of the pelagic Sargassum spp. biomass, J. Environ. Manag. 303 (2022), https://doi.org/10.1016/j.jenvman.2021.114258.
[17] M.P. Tinoco, É.M. de Mendonça, L.I.C. Fernandez, L.R. Caldas, O.A.M. Reales, R.D. Toledo Filho, Life cycle assessment (LCA) and environmental sustainability of cementitious materials for 3D concrete printing: a systematic literature review, J. Build. Eng. 52 (2022), https://doi.org/10.1016/j.jobe.2022.104456.
[18] L. Shamseer, D. Moher, M. Clarke, D. Ghersi, A. Liberati, M. Petticrew, P. Shekelle, L.A. Stewart, D.G. Altman, A. Booth, A.W. Chan, S. Chang, T. Clifford, K. Dickersin, M. Egger, P.C. Gøtzsche, J.M. Grimshaw, T. Groves, M. Helfand, J. Higgins, T. Lasserson, J. Lau, K. Lohr, J. McGowan, C. Mulrow, M. Norton, M. Page, M. Sampson, H. Schünemann, I. Simera, W. Summerskill, J. Tetzlaff, T.A. Trikalinos, D. Tovey, L. Turner, E. Whitlock, Preferred reporting items for systematic review and meta-analysis protocols (prisma-p) 2015: Elaboration and explanation, BMJ 349 (2015) 1–25, https://doi.org/10.1136/bmj.g7647.
[19] V.L. Silva, N. Sanjuán, Opening up the black box: a systematic literature review of life cycle assessment in alternative food processing technologies, J. Food Eng. 250 (2019) 33–45, https://doi.org/10.1016/j.jfoodeng.2019.01.010.
[20] O. Faraji, K. Asiaei, Z. Rezaee, N. Bontis, E. Dolatzarei, Mapping the conceptual structure of intellectual capital research: a co-word analysis, J. Innov. Knowl. 7 (2022), https://doi.org/10.1016/j.jik.2022.100202.
[21] B. Panda, S.C. Paul, L.J. Hui, Y.W.D. Tay, M.J. Tan, Additive manufacturing of geopolymer for sustainable built environment, J. Clean. Prod. 167 (2017) 281–288, https://doi.org/10.1016/j.jclepro.2017.08.165.
[22] B. Panda, S. Chandra Paul, M. Jen Tan, Anisotropic mechanical performance of 3D printed fiber reinforced sustainable construction material, Mater. Lett. 209 (2017) 146–149, https://doi.org/10.1016/j.matlet.2017.07.123.
[23] B. Panda, M.J. Tan, Experimental study on mix proportion and fresh properties of fly ash based geopolymer for 3D concrete printing, Ceram. Int. 44 (2018) 10258–10265, https://doi.org/10.1016/j.ceramint.2018.03.031.
[24] B. Panda, S.C. Paul, N.A.N. Mohamed, Y.W.D. Tay, M.J. Tan, Measurement of tensile bond strength of 3D printed geopolymer mortar, Meas. J. Int. Meas. Confed. 113 (2018) 108–116, https://doi.org/10.1016/j.measurement.2017.08.051.
[25] B. Panda, C. Unluer, M.J. Tan, Investigation of the rheology and strength of geopolymer mixtures for extrusion-based 3D printing, Cem. Concr. Compos. 94 (2018) 307–314, https://doi.org/10.1016/j.cemconcomp.2018.10.002.
[26] J.H. Lim, B. Panda, Q.C. Pham, Improving flexural characteristics of 3D printed geopolymer composites with in-process steel cable reinforcement, Construct. Build. Mater. 178 (2018) 32–41, https://doi.org/10.1016/j.conbuildmat.2018.05.010.
[27] B. Nematollahi, M. Xia, J. Sanjayan, P. Vijay, Effect of type of fiber on inter-layer bond and flexural strengths of extrusion-based 3D printed geopolymer, Mater. Sci. Forum 939 (2018) 155–162, https://doi.org/10.4028/www.scientific.net/MSF.939.155.
[28] R.A. Buswell, W.R. Leal de Silva, S.Z. Jones, J. Dirrenberger, 3D printing using concrete extrusion: a roadmap for research, Cement Concr. Res. 112 (2018) 37–49, https://doi.org/10.1016/j.cemconres.2018.05.006.
[29] W.J. Long, J.L. Tao, C. Lin, Y. cun Gu, L. Mei, H.B. Duan, F. Xing, Rheology and buildability of sustainable cement-based composites containing micro-crystalline cellulose for 3D-printing, J. Clean. Prod. 239 (2019) 118054, https://doi.org/10.1016/j.jclepro.2019.118054.
[30] P. Perez-Cortes, J.I. Escalante-Garcia, Design and optimization of alkaline binders of limestone-metakaolin – a comparison of strength, microstructure and sustainability with portland cement and geopolymers, J. Clean. Prod. 273 (2020) 123118, https://doi.org/10.1016/j.jclepro.2020.123118.
[31] P. Perez-Cortes, J.I. Escalante-Garcia, Alkali activated metakaolin with high limestone contents – Statistical modeling of strength and environmental and cost analyses, Cem. Concr. Compos. 106 (2020) 103450, https://doi.org/10.1016/j.cemconcomp.2019.103450.
[32] K. Korniejenko, P. Kejzlar, P. Louda, The influence of the material structure on the mechanical properties of geopolymer composites reinforced with short fibers obtained with additive technologies, Int. J. Mol. Sci. 23 (2022), https://doi.org/10.3390/ijms23042023.
[33] S. Al-Qutaifi, A. Nazari, A. Bagheri, Mechanical properties of layered geopolymer structures applicable in concrete 3D-printing, Construct. Build. Mater. 176 (2018) 690–699, https://doi.org/10.1016/j.conbuildmat.2018.04.195.
[34] K. Korniejenko, M. Łach, S.Y. Chou, W.T. Lin, A. Cheng, M. Hebdowska-Krupa, S. Gadek, J. Mikuła, Mechanical properties of short fiber-reinforced geopolymers made by casted and 3D printing methods: a comparative study, Materials 13 (2020), https://doi.org/10.3390/ma13030579.
[35] N. Ranjbar, M. Mehrali, C. Kuenzel, C. Gundlach, D.B. Pedersen, A. Dolatshahi-Pirouz, J. Spangenberg, Rheological characterization of 3D printable geopolymers, Cement Concr. Res. 147 (2021) 106498, https://doi.org/10.1016/j.cemconres.2021.106498.
[36] B. Panda, C. Unluer, M.J. Tan, Extrusion and rheology characterization of geopolymer nanocomposites used in 3D printing, Composites, Part B 176 (2019) 107290, https://doi.org/10.1016/j.compositesb.2019.107290.
[37] B. Panda, G.B. Singh, C. Unluer, M.J. Tan, Synthesis and characterization of one-part geopolymers for extrusion based 3D concrete printing, J. Clean. Prod. 220 (2019) 610–619, https://doi.org/10.1016/j.jclepro.2019.02.185.
[38] S.H. Bong, M. Xia, B. Nematollahi, C. Shi, Ambient temperature cured 'just-add-water' geopolymer for 3D concrete printing applications, Cem. Concr. Compos. 121 (2021) 104060, https://doi.org/10.1016/j.cemconcomp.2021.104060.
[39] S. Muthukrishnan, S. Ramakrishnan, J. Sanjayan, Set on demand geopolymer using print head mixing for 3D concrete printing, Cem. Concr. Compos. 128 (2022) 104451, https://doi.org/10.1016/j.cemconcomp.2022.104451.

[40] K. Pasupathy, S. Ramakrishnan, J. Sanjayan, 3D concrete printing of eco-friendly geopolymer containing brick waste, Cem. Concr. Compos. 138 (2023) 104943, https://doi.org/10.1016/j.cemconcomp.2023.104943.

[41] S.H. Bong, B. Nematollahi, V.N. Nerella, V. Mechtcherine, Method of formulating 3D-printable strain-hardening alkali-activated composites for additive construction, Cem. Concr. Compos. 134 (2022) 104780, https://doi.org/10.1016/j.cemconcomp.2022.104780.

[42] M.V. Tran, T.H. Vu, T.H.Y. Nguyen, Simplified assessment for one-part 3D-printable geopolymer concrete based on slump and slump flow measurements, Case Stud. Constr. Mater. 18 (2023) e01889, https://doi.org/10.1016/j.cscm.2023.e01889.

[43] S. Muthukrishnan, S. Ramakrishnan, J. Sanjayan, Effect of alkali reactions on the rheology of one-part 3D printable geopolymer concrete, Cem. Concr. Compos. 116 (2021) 103899, https://doi.org/10.1016/j.cemconcomp.2020.103899.

[44] S. Muthukrishnan, S. Ramakrishnan, J. Sanjayan, Effect of microwave heating on interlayer bonding and buildability of geopolymer 3D concrete printing, Construct. Build. Mater. 265 (2020) 120786, https://doi.org/10.1016/j.conbuildmat.2020.120786.

[45] A. Bagheri, C. Cremona, Formulation of mix design for 3D printing of geopolymers: a machine learning approach, Mater. Adv. 1 (2020) 720–727, https://doi.org/10.1039/d0ma00036a.

[46] X. Guo, J. Yang, G. Xiong, Influence of supplementary cementitious materials on rheological properties of 3D printed fly ash based geopolymer, Cem. Concr. Compos. 114 (2020) 103820, https://doi.org/10.1016/j.cemconcomp.2020.103820.

[47] S.H. Bong, B. Nematollahi, A. Nazari, M. Xia, J.G. Sanjayan, Fresh and Hardened Properties of 3D Printable Geopolymer Cured in Ambient Temperature, Springer International Publishing, 2019, https://doi.org/10.1007/978-3-319-99519-9_1.

[48] S.H. Bong, B. Nematollahi, A. Nazari, M. Xia, J. Sanjayan, Method of optimisation for ambient temperature cured sustainable geopolymers for 3D printing construction applications, Materials 16 (2019), https://doi.org/10.3390/ma12060902.

[49] Z. Li, L. Wang, G. Ma, Mechanical improvement of continuous steel microcable reinforced geopolymer composites for 3D printing subjected to different loading conditions, Composites, Part B 187 (2020) 107796, https://doi.org/10.1016/j.compositesb.2020.107796.

[50] A. Kashani, T. Ngo, Optimisation of mixture properties for 3D printing of geopolymer concrete - Department of infrastructure Engineering, the university of Melbourne, Australia, Proc. 35th Int. Symp. Autom. Robot. Constr. (2018), https://doi.org/10.22260/ISARC2018/0037.

[51] M. Valente, M. Sambucci, M. Chougan, S.H. Ghaffar, Composite alkali-activated materials with waste tire rubber designed for additive manufacturing: an eco-sustainable and energy saving approach, J. Mater. Res. Technol. 24 (2023) 3098–3117, https://doi.org/10.1016/j.jmrt.2023.03.213.

[52] M. Chougan, S. Hamidreza Ghaffar, M. Jahanzat, A. Albar, N. Mujaddedi, R. Swash, The influence of nano-additives in strengthening mechanical performance of 3D printed multi-binder geopolymer composites, Construct. Build. Mater. 250 (2020) 118928, https://doi.org/10.1016/j.conbuildmat.2020.118928.

[53] A. Albar, M. Chougan, M.J. Al- Kheetan, M.R. Swash, S.H. Ghaffar, Effective extrusion-based 3D printing system design for cementitious-based materials, Results Eng 6 (2020), https://doi.org/10.1016/j.rineng.2020.100135.

[54] M. Chougan, S.H. Ghaffar, P. Sikora, S.Y. Chung, T. Rucinska, D. Stephan, A. Albar, M.R. Swash, Investigation of additive incorporation on rheological, microstructural and mechanical properties of 3D printable alkali-activated materials, Mater. Des. 202 (2021), https://doi.org/10.1016/j.matdes.2021.109574.

[55] H. Alghamdi, S.A.O. Nair, N. Neithalath, Insights into material design, extrusion rheology, and properties of 3D-printable alkali-activated fly ash-based binders, Mater. Des. 167 (2019) 107634, https://doi.org/10.1016/j.matdes.2019.107634.

[56] H. Alghamdi, N. Neithalath, Synthesis and characterization of 3D-printable geopolymeric foams for thermally efficient building envelope materials, Cem. Concr. Compos. 104 (2019) 103377, https://doi.org/10.1016/j.cemconcomp.2019.103377.

[57] X. Lv, Y. Qin, H. Liang, X. Cui, Effects of modifying agent on rheology and workability of alkali-activated slag paste for 3D extrusion forming, Construct. Build. Mater. 302 (2021) 124062, https://doi.org/10.1016/j.conbuildmat.2021.124062.

[58] B. Panda, S. Ruan, C. Unluer, M.J. Tan, Investigation of the properties of alkali-activated slag mixes involving the use of nanoclay and nucleation seeds for 3D printing, Composites, Part B 186 (2020) 107826, https://doi.org/10.1016/j.compositesb.2020.107826.

[59] C. Sun, J. Xiang, M. Xu, Y. He, Z. Tong, X. Cui, 3D extrusion free forming of geopolymer composites: materials modification and processing optimization, J. Clean. Prod. 258 (2020) 120986, https://doi.org/10.1016/j.jclepro.2020.120986.

[60] D.W. Zhang, D. min Wang, X.Q. Lin, T. Zhang, The study of the structure rebuilding and yield stress of 3D printing geopolymer pastes, Construct. Build. Mater. 184 (2018) 575–580, https://doi.org/10.1016/j.conbuildmat.2018.06.233.

[61] M. Tramontin Souza, L. Simão, E. Guzi de Moraes, L. Senff, J.R. de Castro Pessôa, M.J. Ribeiro, A.P. Novaes de Oliveira, Role of temperature in 3D printed geopolymers: evaluating rheology and buildability, Mater. Lett. 293 (2021) 129680, https://doi.org/10.1016/j.matlet.2021.129680.

[62] J. Archez, N. Texier-Mandoki, X. Bourbon, J.F. Caron, S. Rossignol, Shaping of geopolymer composites by 3D printing, J. Build. Eng. 34 (2021) 101894, https://doi.org/10.1016/j.jobe.2020.101894.

[63] J. Archez, S. Maitenaz, L. Demont, M. Charrier, R. Mesnil, N. Texier-Mandoki, X. Bourbon, S. Rossignol, J.F. Caron, Strategy to shape, on a half-meter scale, a geopolymer composite structure by additive manufacturing, Open Ceram 5 (2021) 100071, https://doi.org/10.1016/j.oceram.2021.100071.

[64] S. Ma, S. Fu, S. Zhao, P. He, G. Ma, M. Wang, D. Jia, Y. Zhou, Direct ink writing of geopolymer with high spatial resolution and tunable mechanical properties, Addit. Manuf. 46 (2021) 102202, https://doi.org/10.1016/j.addma.2021.102202.

[65] S. Ma, H. Yang, S. Zhao, P. He, Z. Zhang, X. Duan, Z. Yang, D. Jia, Y. Zhou, 3D-printing of architectured short carbon fiber-geopolymer composite, Composites, Part B 226 (2021) 109348, https://doi.org/10.1016/j.compositesb.2021.109348.

[66] M.B. Jaji, K.A. Ibrahim, G.P.A.G. van Zijl, A.J. Babafemi, Thixotropic characterisation of slag modified 3D printable metakaolin based geopolymer composite, Mater. Today Proc. (2023), https://doi.org/10.1016/j.matpr.2023.03.530, 0–6.

[67] O. Şahin, H. İlcan, A.T. Ateşli, A. Kul, G. Yıldırım, M. Şahmaran, Construction and demolition waste-based geopolymers suited for use in 3-dimensional additive manufacturing, Cem. Concr. Compos. 121 (2021), https://doi.org/10.1016/j.cemconcomp.2021.104088.

[68] H. Ilcan, O. Sahin, A. Kul, G. Yildirim, M. Sahmaran, Rheological properties and compressive strength of construction and demolition waste-based geopolymer mortars for 3D-Printing, Construct. Build. Mater. 328 (2022) 127114, https://doi.org/10.1016/j.conbuildmat.2022.127114.

[69] Q. Munir, R. Peltonen, T. Kärki, Printing parameter requirements for 3d printable geopolymer materials prepared from industrial side streams, Materials 14 (2021), https://doi.org/10.3390/ma14164758.

[70] A. Bajpayee, M. Farahbakhsh, U. Zakira, A. Pandey, L.A. Ennab, Z. Rybkowski, M.K. Dixit, P.A. Schwab, N. Kalantar, B. Birgisson, S. Banerjee, In situ Resource utilization and Reconfiguration of soils into construction materials for the additive manufacturing of buildings, Front. Mater. 7 (2020) 1–12, https://doi.org/10.3389/fmats.2020.00052.

[71] A. Hasnaoui, E. Ghorbel, G. Wardeh, Optimization approach of granulated blast furnace slag and metakaolin based geopolymer mortars, Construct. Build. Mater. 198 (2019) 10–26, https://doi.org/10.1016/j.conbuildmat.2018.11.251.

[72] International Energy Agency - IAE, Coal 2020 - Analysis and Forecast to 2025, 2020.

[73] Australian Government, Department of climate change, energy, the environment and water, Electricity generation. https://www.energy.gov.au/data/electricity-generation, 2022. (Accessed 18 April 2023).

[74] P.H.R. Borges, N. Banthia, H.A. Alcamand, W.L. Vasconcelos, E.H.M. Nunes, Performance of blended metakaolin/blastfurnace slag alkali-activated mortars, Cem. Concr. Compos. 71 (2016) 42–52, https://doi.org/10.1016/j.cemconcomp.2016.04.008.

[75] B. Nematollahi, P. Vijay, J. Sanjayan, A. Nazari, M. Xia, V.N. Nerella, V. Mechtcherine, Effect of polypropylene fibre addition on properties of geopolymers made by 3D printing for digital construction, Materials 11 (2018), https://doi.org/10.3390/ma11122352.

[76] S. Kumar, R. Kumar, S.P. Mehrotra, Influence of granulated blast furnace slag on the reaction, structure and properties of fly ash based geopolymer, J. Mater. Sci. 45 (2010) 607–615, https://doi.org/10.1007/s10853-009-3934-5.

[77] J.L. Provis, J.S.J. Van Deventer, Geopolymers and Other Alkali-Activated Materials, fifth ed., Elsevier Ltd., 2019 https://doi.org/10.1016/B978-0-08-100773-0.00016-2.

[78] J.G.S. Van Jaarsveld, J.S.J. Van Deventer, Effect of the alkali metal activator on the properties of fly ash-based geopolymers, Ind. Eng. Chem. Res. 38 (1999) 3932–3941, https://doi.org/10.1021/ie980804b.

[79] R. Tänzer, Y. Jin, D. Stephan, Alkali activated slag binder: effect of cations from silicate activators, Mater. Struct. Constr. 50 (2017), https://doi.org/10.1617/s11527-016-0961-y.
[80] M. Król, P. Rożek, D. Chlebda, W. Mozgawa, Influence of alkali metal cations/type of activator on the structure of alkali-activated fly ash – ATR-FTIR studies, Spectrochim. Acta Part A Mol. Biomol. Spectrosc. 198 (2018) 33–37, https://doi.org/10.1016/j.saa.2018.02.067.
[81] M. Sitarz, J. Castro-Gomes, I. Hager, Strength and microstructure characteristics of blended fly ash and ground granulated blast furnace slag geopolymer mortars with na and K silicate solution, Materials 15 (2022), https://doi.org/10.3390/ma15010211.
[82] J. Christ, S. Leusink, H. Koss, Multi-axial 3D printing of biopolymer-based concrete composites in construction, Mater. Des. 235 (2023) 112410, https://doi.org/10.1016/j.matdes.2023.112410.
[83] S. El-Sayegh, L. Romdhane, S. Manjikian, A critical review of 3D printing in construction: benefits, challenges, and risks, Arch. Civ. Mech. Eng. 20 (2020) 1–25, https://doi.org/10.1007/s43452-020-00038-w.
[84] J. Sun, W. Zhou, L. Yan, D. Huang, L. ya Lin, Extrusion-based food printing for digitalized food design and nutrition control, J. Food Eng. 220 (2018) 1–11, https://doi.org/10.1016/j.jfoodeng.2017.02.028.
[85] M. Xia, B. Nematollahi, J. Sanjayan, Influence of binder saturation level on compressive strength and dimensional accuracy of powder-based 3D printed geopolymer, Mater. Sci. Forum 939 (2018) 177–183, https://doi.org/10.4028/www.scientific.net/MSF.939.177.
[86] M. Xia, B. Nematollahi, J. Sanjayan, Printability, accuracy and strength of geopolymer made using powder-based 3D printing for construction applications, Autom. ConStruct. 101 (2019) 179–189, https://doi.org/10.1016/j.autcon.2019.01.013.
[87] V. Voney, P. Odaglia, C. Brumaud, B. Dillenburger, G. Habert, From casting to 3D printing geopolymers: a proof of concept, Cement Concr. Res. 143 (2021) 106374, https://doi.org/10.1016/j.cemconres.2021.106374.
[88] M. Xia, J.G. Sanjayan, Methods of enhancing strength of geopolymer produced from powder-based 3D printing process, Mater. Lett. 227 (2018) 281–283, https://doi.org/10.1016/j.matlet.2018.05.100.
[89] S. Liu, B. Lu, H. Li, Z. Pan, J. Jiang, S. Qian, A comparative study on environmental performance of 3D printing and conventional casting of concrete products with industrial wastes, Chemosphere 298 (2022) 134310, https://doi.org/10.1016/j.chemosphere.2022.134310.
[90] R. Robayo-Salazar, J. Mejía-Arcila, R. Mejía de Gutiérrez, E. Martínez, Life cycle assessment (LCA) of an alkali-activated binary concrete based on natural volcanic pozzolan: a comparative analysis to OPC concrete, Construct. Build. Mater. 176 (2018) 103–111, https://doi.org/10.1016/j.conbuildmat.2018.05.017.
[91] M. Fawer, M. Concannon, W. Rieber, Life cycle inventories for the production of sodium silicates, Int. J. Life Cycle Assess. 4 (1999) 207–212, https://doi.org/10.1007/BF02979498.
[92] European IPPC Bureau, Integrated Pollution Prevention and Control - Reference Document on Best Available Techniques for the Manufacture of Large Volume Inorganic Chemicals, Solids and Others Industry, Brussels, Belgium, 2007.
[93] J. Payá, F. Agrela, J. Rosales, M.M. Morales, M.V. Borrachero, Application of alkali-activated industrial waste, in: F.A. Jorge de Brito (Ed.), Woodhead Publ. Ser. Civ. Struct. Eng. New Trends Eco-Efficient Recycl. Concr., Woodhead Publishing, 2018, pp. 357–424, https://doi.org/10.1016/B978-0-08-102480-5.00013-0.
[94] National Standards Authority of Ireland (NSAI), NSAI calls for public comment on ISO/ASTM DIS 52939 - Additive Manufacturing for Construction. https://www.nsai.ie/about/news/iso-astm-dis-52939-additive-manufacturing-for-construction/. Last accessed: May.15.2023..
[95] The Heinrich Böll Foundation, Energía en América Latina, 2019. https://br.boell.org/sites/default/files/2020-01/EnergíaenAméricaLatina_Factsheet_2019_3.pdf. (Accessed 10 March 2023).
[96] M.H. Raza, R.Y. Zhong, M. Khan, Recent advances and productivity analysis of 3D printed geopolymers, Addit. Manuf. 52 (2022) 102685, https://doi.org/10.1016/j.addma.2022.102685.
[97] G. Lazorenko, A. Kasprzhitskii, Geopolymer additive manufacturing : a review, Addit. Manuf. 55 (2022) 102782, https://doi.org/10.1016/j.addma.2022.102782.
[98] M. Amran, H.S. Abdelgader, A.M. Onaizi, R. Fediuk, T. Ozbakkaloglu, R.S.M. Rashid, G. Murali, 3 D-printable alkali-activated concretes for building applications : a critical review, Construct. Build. Mater. 319 (2022) 126126, https://doi.org/10.1016/j.conbuildmat.18882021.126126.
[99] S. Qaidi, A. Yahia, B.A. Tayeh, H. Unis, R. Faraj, Mohammed Ahmed, 3D printed geopolymer composites: a review, Mater. Today Sustain. 95 (2022) 106408, https://doi.org/10.1016/j.mtsust.2022.100240.
[100] S. Luhar, I. Luhar, The Open Construction & Building Additive Manufacturing in the Geopolymer Construction Technology : A Review, 2020, pp. 150–161, https://doi.org/10.2174/1874836802014010150.